INTRACELLULAR DELIVERY OF DENDRIMER-BASED NANOCONJUGATES FOR CANCER AND NEUROINFLAMMATION

by
Jiangyu Li

A thesis submitted to Johns Hopkins University in conformity with the requirements for the degree of Master of Science in Engineering

Baltimore, Maryland

May, 2016

Abstract

Activated microglia/macrophages have been implicated as key players in many central nervous system (CNS) diseases, such as brain tumor and Rett syndrome, in which they secrete regulatory/inflammatory cytokines that either suppress the local immune activity or lead to neurodegeneration, respectively. Polyamidoamine (PAMAM) dendrimers have been shown as promising nanodevices that specifically target activated microglia/macrophages in both brain tumor and Rett syndrome. Understanding the effects of dendrimer-drug conjugates on activated microglia/macrophages on a cellular level may provide guidance toward the improvement of *in vivo* efficacy in these diseases. Colony stimulating factor 1 (CSF1), mitogen-activated protein kinases (MAPKs) and glutaminase (GLS) are potential targets to modulate neuroinflammatory properties. In this study, we developed PAMAM dendrimer-conjugated inhibitors against CSF1 receptor (D-BLZ945), MAPKs (D-PD98059) and GLS (D-JHU29), and tested the *in vitro* efficacies in different microglia cell lines, BV2 and/or Raw 264.7. D-BLZ945 and D-JHU29 did not exhibit cytotoxicity and had better or similar efficacy compared to free BLZ945 and JHU29. However, D-PD98059 didn't demonstrate improved therapeutic effect compared to free PD98059. Given the ability of dendrimers to target activated microglia, D-BLZ945 and D-JHU29 may have improved potential for treating inflammation compared to free drugs. This study indicates that dendrimer conjugates have comparative efficacy to free drugs on cellular level with increased drug solubility.

Advisor: Rangaramanujam Kannan, Ph.D.

Thesis Committee: Rangaramanujam Kannan, Ph.D.; Laura Ensign, Ph.D.; Sujatha Kannan, M.D.

Acknowledgments

First of all, I would like to express my deepest gratitude to my advisor, Professor Rangaramanujam M. Kannan of the Department of Ophthalmology at Johns Hopkins School of Medicine. I appreciate this precious opportunity Dr. Kannan gives me to learn and to do research in the lab. It is his wise guidance, motivation and constant support that enable me to finish this research project and put this thesis together. The door to Dr. Kannan's office was always open whenever I had a question about my research or writing. His enthusiasm, wisdom and charming personality illuminated me a lot and gave me confidence facing the challenges during the study.

Besides my advisor, I would like to express my sincere gratitude to the members of my thesis committee: Professors Sujatha Kannan and Laura Ensign, for generously offering time and support to review my thesis.

I would like to express my special thanks to Drs. Rajsekhar R. Ramireddy and Fan Zhang for training me on experimental techniques, helping me with my projects and giving me advices for thesis writing patiently and kindly. I also want to thank Drs. Siva Kambhampati, Jongsung Park and Soo-Young Kim for their kindly guidance for my project and writing. Their help was vital for me to accomplish this study. I would like to thank my lab fellows in the Center for Nanomedicine for their kind help, encouragement and friendship. I feel very grateful that I was able to be part of such an amazing lab.

I would also like to thank my families and friends to give me support and encouragement throughout my master study.

Table of Contents

List of Figures

List of Tables

Chapter 1: Introduction

1.1 PAMAM dendrimers as potent drug delivery vehicles

Dendrimers are repetitively branched molecules that have been recently used as nanocarrier system for drug delivery.[1] Polyamidoamine (PAMAM) dendrimers are a class of dendrimer with hyperbranched units of amide and amine. There are multiple properties that make dendrimers favorable delivery vehicles: (1) Small and controllable size: The sizes of most generations of PAMAM dendrimers are within nanoscale (1 to 10 nm in diameter) as shown in **Figure 1**. As the number of dendrimer generations or layers increases, dendrimer diameter increases about 1 nm per layer and the number of surface functional groups increases exponentially.[2] MRI imaging shows that G = 3 to 9 PAMAM dendrimers sizes are in the range to preclude extravasation, making them great blood pool agents compared to Magnevist which completely excreted through kidney.[3] (2) Modifiable surface functional groups: By varying terminal groups, dendrimers can be cationic (-NH2 terminated), neutral (-OH terminated) or anionic (-COOH terminated). Dendrimers with different surface groups have distinct endocytosis mechanism and could target specific intracellular compartments.[4] Compared to linear poylmers, dendrimers have abundant surface reactive groups and high surface area to volume ratio, which make them promising carriers with high drug payload. They can be loaded with bioactive molecules either by covalent conjugation or encapsulation through inner void space.[3]

(3) Biocompatibility: Dendrimer toxicity is associated with its size/generation and surface charge. Generally, PAMAM dendrimers with smaller size, neutral and anionic surface charge

would exhibit less toxic and lower permeation. PEG-layered PAMAM dendrimers are examples of biocompatible and degradable dendrimers which have enhanced permeation and retention (EPR).[5,6,7] (4) Ability to overcome biological barrier and intrinsic property of targeting activated microglial cells. Evidence showed that PAMAM dendrimers could across the blood brain barrier (BBB) to deliver drug into malignant gliomas cells.[8] Hydroxyl-functionalized PAMAM dendrimers could selectively targeted in the injured neurons and brain microglia cells using systemic administration.[9] Confocal imaging illustrates the rapid and selective distribution of dendrimer-Cy5 conjugates in solid brain tumor, followed by retention in tumor-associated microglia.[10] Dendrimer has also shown to target activated microglia cells in injured mouse Retina upon intravitreal injection.[11] These properties enable PAMAM dendrimers to be promising candidates for delivering unstable and hydrophobic drugs into central nervous system.

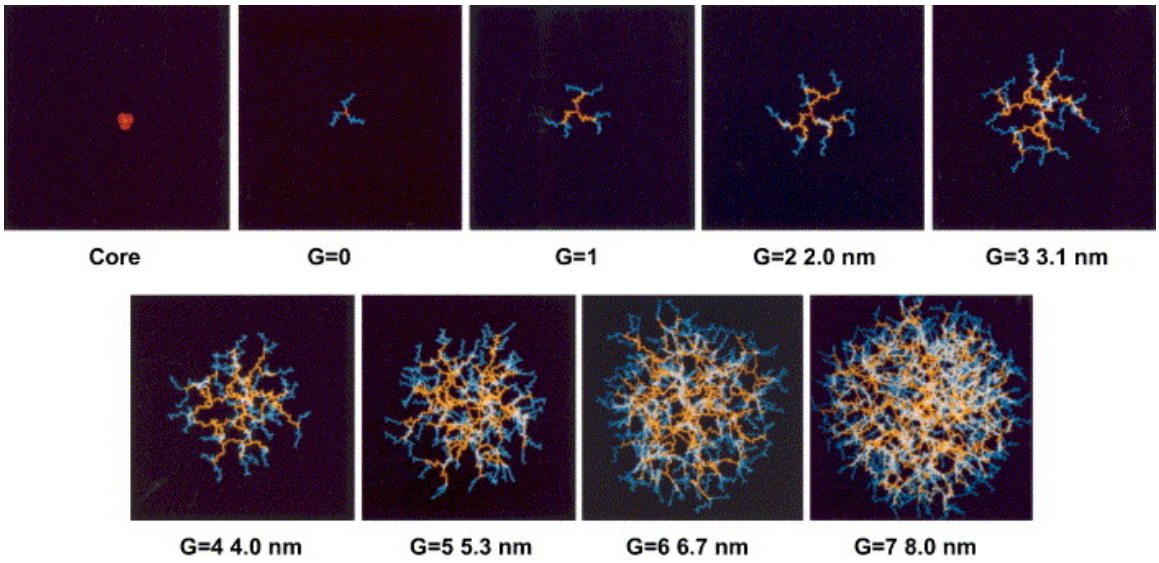

Figure 1 Size and shape of PAMAM dendrimer from core to generation G=7. [2]

1.2 Role and characterization of tumor associated macrophages (TAMs)

Tumor associate macrophages (TAMs) are leukocyte population mainly found in the tumor microenvironment, contributing to tumor initiation, progression and metastasis.[12] Macrophages polarize into different functional forms in response to local cytokine signals. One widely accepted theory differentiates the distinct macrophage functional states into classically activated M1 phenotype and alternatively activated M2 phenotype.[13] M1 macrophages highly express pro-inflammatory cytokines, leading to pathogen killing, tissue damage and inflammation.[14] In contrast, M2 macrophages secrete more anti-inflammatory cytokines, which are thought to facilitate neovascularization and tumor growth.[15] There is no consensus on the relative importance of M1 and M2 macrophages in tumor development. At the tumor initiating stage, macrophages produce cytokines and growth factors such as interleukin-6 (IL-6), tumor necrosis factor-α (TNF-α), and interferon-γ (IFN-γ), generating chronic inflammatory responses.[16] After tumors are established, the microenvironment turned from pro-inflammation into anti-inflammation. Macrophages are polarized by IL4 secreted from CD4+ T cells, as well as colony stimulating factor-1 (CSF1) and GM-CSF from tumor cells.[16]

M1 and M2 phenotypes are featured by different signaling pathway activation and distinct expression level of surface receptors and cytokines. Stimulated by IFN-γ and LPS or TNF-α, M1 macrophages express higher level of IL-12, IL-23 and tumor necrosis factor (TNF). [13, 14] M1 macrophages also up-regulate inducible nitric oxide synthase (iNOS) activation to release high concentration of nitric oxide (NO) (**Figure 2**).[17] NO is considered to be a pro-inflammatory agent due to its ability to induce inflammation and toxic reactions against infection and other tissues.[18] By comparison, Immune complexes (ICs), IL4 and IL-13, IL-

10, TGFβ and macrophage colony stimulating factor (MCSF) polarize macrophages to be M2 phenotype.[13, 14] M2 macrophages have high IL-10 expression and generate low level of IL-12. Instead of iNOS activation, it is arginase pathway that predominates in the M2 subsets (**Figure 2**).[19] High arginase 1(the liver isoform of arginase) production is a distinct feature for M2 macrophages. The up-regulation of arginase inhibits the translation of NO synthase 2 (NOS2) mRNA.[20] It halts the production of NO released by NOS2, which is a potential anti-inflammatory mechanism [17]. The increased Arginase 1 production is transcribed by STAT6, a downstream signaling molecule of IL4/IL-13 receptor pathway.[21]

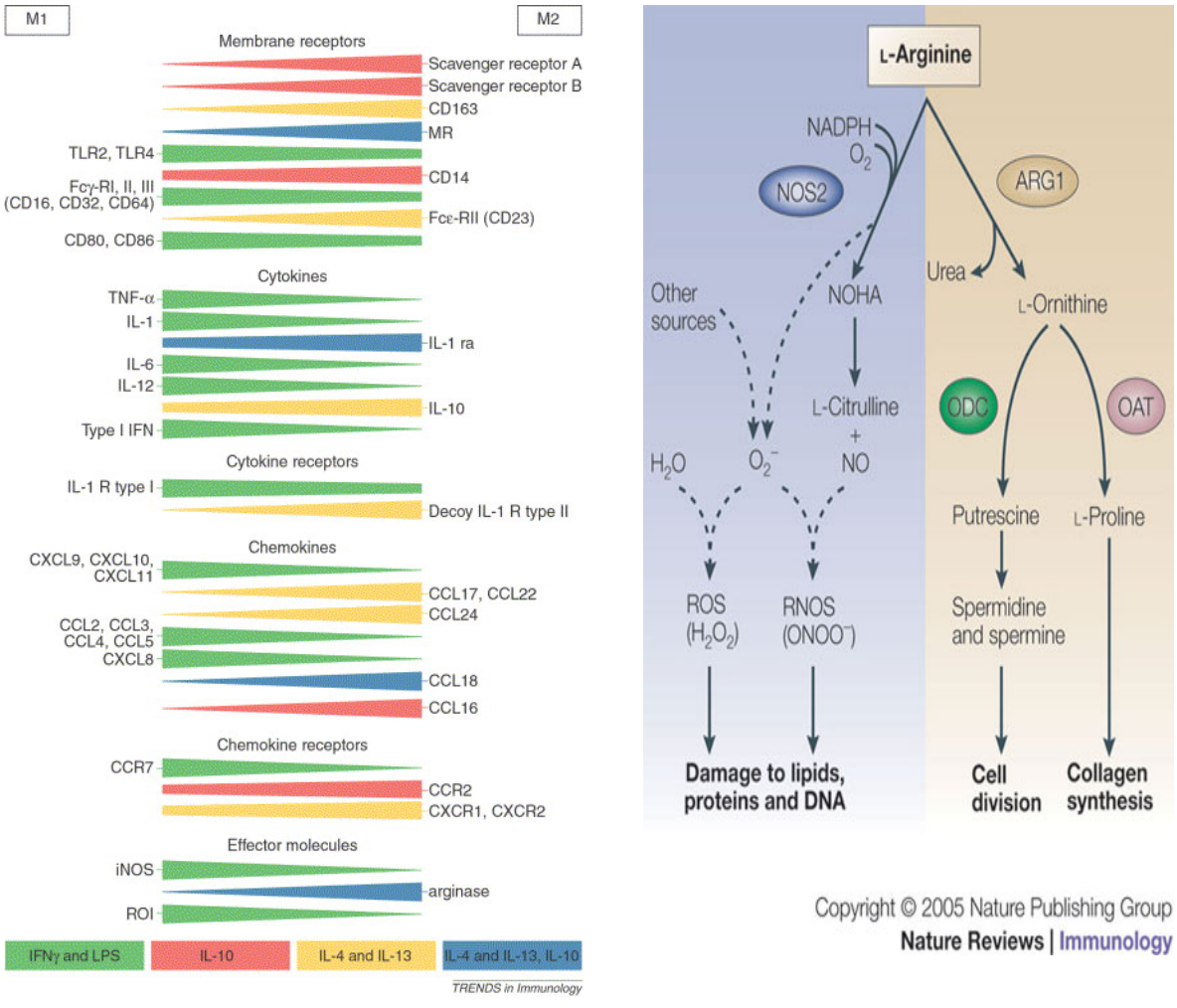

Figure 2 Key features for M1 and M2 macrophages.[17, 19]

1.3 CSF1/CSF1R pathway role in tumor

CSF1, also called macrophage-colony stimulating factor (M-CSF), is a main hematopoietic cytokine regulating most macrophages and is significantly involved in the recruiting of macrophages into tumors by facilitating migration and survival.[22] The activation of CSF1R stimulates gene expression and cytoskeletal remodeling, which leads to the mediation of target cell proliferation and differentiation.[23] M2 type macrophages in primary tumors facilitate tumor cell invasion through an interaction involving tumor-secreted CSF1 and macrophage-synthesized EGF that mediates tumor migration along collagen fibers to blood vessels.[16] The bind of CSF1 to its receptor (CSF1R) would activate the phosphorylation cascade of CSF1R and downstream molecules. One example is phosphorylating PIK3R1 that regulates phosphatidylinositol 3-kinase (PI3K), resulting in the activation of PI3K-Akt1 signaling pathway.[24] Activated CSF1R initiates the activation of the PI3K-Akt1 pathway, MAPK/ERK pathway and signal transducer and activator of transcription(STAT) family memberes STAT3, STAT5A and/or STAT5B.[24]

Due to its critical role in regulating macrophages survival and activation (**Figure 3**), CSF1 is an important factor in innate immunity and is involved in the pathology underlying various diseases[23]. Evidences showed that the tumor infiltration process of CD8+ T cells was increased and the tumor growth rates in both mammary and cervical tumor model were attenuated after inhibiting CSF1/CSF1R pathway.[25, 26] There are twelve clinical trials currently undergoing for therapeutic regents with the target of CSF1/CSF1R pathway in multiple cancers, such as breast carcinoma, leukemia, and glioblastoma.[26]

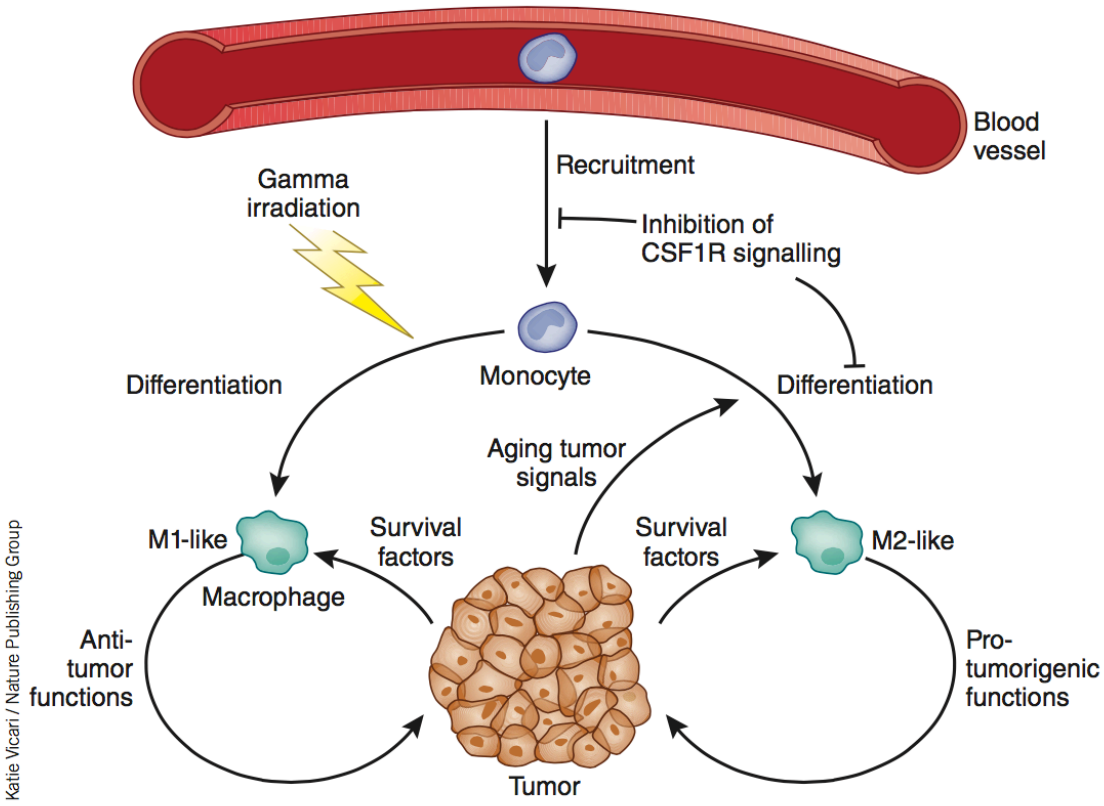

Figure 3 Role of CSF1 in polarization of TAMs. Monocyte differentiates into M1 or M2-like macrophage after receiving distinct signals. M1 subtype macrophages exhibit anti-tumor functions whereas M2 subtype macrophages exhibit pro-tumorigenic functions. Inhibition of CSF1R signaling reduces the recruitment of TAMs and halts the polarization of M2-like macrophages. [15]

1.4 MAPK pathway role in tumor and inflammation

Mitogen-activated protein kinases (MAPKs) are essential enzymes for transducing signals from surface receptor to genes. This process initiates cellular responses to stimuli and mediates cell proliferation, differentiation and apoptosis.[27] The MAPK cascades consist of MAPK, MAPK kinase (MAPKK or MEK) and MAPKK kinases (MAPKKK or MEKK). Phosphorylation of MAPK cascades and substrate proteins controls the activation of downstream transcription factors and cytoskeletal proteins.[28] There are three well-characterized subfamilies of MAPKs: the extracellular signal–regulated kinases (ERKs); the c-Jun NH2-terminal kinases (JNKs) and p38 enzymes. ERKs are essential in controlling cell

division and inhibitors of the ERK pathways are under clinical trials as potential anticancer agents.[29] JNKs are critical regulators of transcription and cell apoptosis. JNKs inhibitors could promote the effect of chemotherapy in inhibiting tumor cell growth. The activation of p38 in immune cells is important in initiating immune response. [29] Considering the fact that ERK, JNK, and p38 pathways are all drug targets, inhibitors of MAPKs are promising drug candidates to treat inflammation, cancer and other diseases.[29] MAPK pathway gets activated in macrophages in response to a variety of stimuli. LPS and tumor necrosis factor-α (TNF-α), for instance, are widely used agents to study MAPKs activation in macrophages. Both of LPS and TNF- α activate all three subfamilies of MAPKs.[30] MAPKs stimulated by inflammatory cytokines and environmental stresses may be the mechanism underling diseases including asthma and autoimmunity [29]. Evidence showed that anthrax lethal toxin inhibits MAPK activation in macrophages and interferes with the secretion of pro-inflammatory cytokines.[31]

1.5 Glutaminase (GLS) role in neuroinflammation

Glutaminase (GLS) is the enzyme localized in mitochondria accelerating the hydrolysis process of glutamine into glutamate and ammonia, which is an important energy source for rapidly proliferating cells like malignant tumor cells.[32] It offers an efficient and alternative way to reprogram cancer cell metabolism under hypoxic conditions.[33] In central nervous system, the overexpression of GLS in macrophages leads to the accumulation of glutamate, an important neurotransmitter. The up-regulated extracellular glutamate level is the mechanism underlying several inflammatory disorders like traumatic brain injury and HIV-1 associated dementia.[34, 35, 36] Glutamate released from activated microglia contributes to the neuron cells injury under inflammatory stimulation.[37] GLS inhibitors could decrease

excessive extracellular glutamate and may be potential therapeutic agents against carcinoma and neuroinflammation.[38]

1.6 Thesis overview

This thesis focused on developing dendrimer mediated therapy for the treatment of glioblastoma and neuroinflammation. Specifically, we evaluated the therapeutic efficacy of dendrimer-drug conjugates on the molecular level. Small molecular drugs with low solubility can be conjugated to PAMAM dendrimer to generate highly soluble dendrimer drug therapeutics with similar or better efficacy compared to free drug in vitro with increased cell uptake. Colony stimulating factor 1 (CSF1), glutaminase (GLS) and Mitogen-activated protein kinases (MAPKs) are potential targets for modulating inflammation progression as described above. Inhibition to these targets might provide therapeutic opportunities in promoting the immunity in brain tumor, and attenuating neuroinflammation in Rett syndrome. The goal of this study is to investigate the potential therapeutic efficacy of dendrimer-drug conjugates for these diseases on activated microglia/macrophages (M1 or M2) at in vitro cellular level. I am trying to achieve this goal with three specific aims listed below.

Specific Aim 1. Synthesize dendrimer-based nano-conjugates for targeting TAMs for more efficacious treatment in 9L glioblastoma model. CSF1 and MAPKs are important factors influencing macrophage polarization and tumor growth. Aiming to modulate TAMs phenotype in tumor microenvironment, CSF1 receptor inhibitor BLZ945 and MAPK pathway inhibitor PD98059 were conjugated to generation four PAMAM dendrimers (G4OH).

Specific Aim 2. Study the therapeutic efficacy of D-BLZ945 and D-PD98059 at the cellular level in vitro. BLZ945 was shown to reduce M2 phenotype cytokines expression in macrophage and had the potential to mediate macrophage polarization. Thus, I evaluated the *in vitro* efficacy of D-BLZ945 in affecting the production of arginase-1 in macrophages, a distinct feature for the M2 phenotype. On the other hand, PD98059 has been widely used as a potent inhibitor to MAPK signaling. Considering the role of MAPKs in pro-inflammatory polarization of macrophage, we assessed the efficacy of D-PD98059 by measuring the pro-inflammatory cytokine expression level.

Specific Aim 3. Evaluate D-JHU29 on its efficacy to inhibit glutaminase enzyme in vitro. JHU29 is a Bis-2-(5-phenylacetamido-1,2,4-thiadiazol-2-yl)ethyl sulfide (BPTES) analog which could inhibit human kidney-type glutaminase with IC_{50} of 2.7 μM. The inhibitory effect of D-JHU29 on extracellular glutamate levels is evaluated in Chapter 4.

Chapter 2: Design and synthesis of D-PD98059 and D-BLZ945 conjugates

2.1 Introduction

Hydroxyl-terminated generation 4 PAMAM dendrimer (G4-OH) has favorable properties including small size (~4 nm), positive surface charge and ability to cross the blood brain barrier.[9] We have shown the dendrimer conjugated N-acetylcysteine (NAC) can be specifically delivered to activated microglial cells in rabbit model of cerebral palsy without the help of targeting ligands.[39] The dendrimer-NAC conjugate was also shown to have more efficacious anti-oxidant and anti-inflammatory effect in vitro.[40] Through a fluorescence-based quantification method, we showed that G4OH dendrimer accumulated in the brain tumor rapidly upon systemic administration and target TAMs gradually in a 9L gliosarcoma model.[10] This targeted accumulation indicates that PAMAM G4OH dendrimer is a promising nano-vehicle in delivering immune-modulatory drugs to TAMs for the treatment of malignant gliomas.[10] Based on these studies, we designed, synthesized D-PD98059 and D-BLZ945 conjugates, and thoroughly characterized the physiochemical properties.

PD98059 is a highly selective inhibitor for MAPK kinase (MEK) in MAPK pathway with IC_{50} of 2 μM in a cell-free assay.[41] PD98059 inhibits MEK1 activation via Raf or MEK kinase (MEKK) with IC_{50} of 4 μM and inhibits MEK2 activation via Raf with IC_{50} of 50 μM.[41] PD98059 was also shown to inhibit the proliferation of murine macrophage RAW264.7 cells in the culture containing nuclear factor kappa B ligand (RANKL) in a dose-dependent manner.[42] However, PD98059 is poorly soluble in water or ethanol (<1 mg/mL). Even in DMSO, PD98059 has a low solubility (14 mg/mL) and requires heating for

solubilization. We envision the possibility that by conjugating PD98059 to the dendrimer, the solubility, targeting capability and therapeutic effect of the drug can be improved. D-PD98059 conjugates were formulated with different synthetic schemes and aimed to attenuate the MEK pathways in macrophages.

Besides MAPK pathway, another more specific target to modifying TAMs polarization is CSF1/CSF1R signaling.[15] CSF1 expressed by tumor cells binds to the CSF1 receptor on the surface of TAMs, resulting in suppressing immune response at tumor sites.[26,43] Several therapeutic agents targeting CSF1R are currently involved in clinical trials, including small molecule inhibitors PLX3397, ARRY-382 and JNJ-40346527 (**Table 1**).[44] However, these small molecule inhibitors are not exclusively targeting CSF1R (**Table 2**).[44,45] By comparison, BLZ945 is a highly potent, and selective inhibitor for Colony Stimulating Factor-1 Receptor (CSF1R), with ~ 1 nM IC_{50} concentrations in cell-free assay (**Table 2**).[46] BLZ945 was shown to inactivate CSF1R phosphorylation and inhibits CSF1-dependent cell proliferation with EC50 of 67 nM.[15,46] It hinders the CSF1/CSF1R signaling between macrophages and glioma cells and breaks the favorable growing environment for tumor by potentially repolarizing the tumor associate macrophages.[16] CSF1R inhibition by BLZ945 is known to reduce tumor growth and progression in PDG mice (Mice expressing platelet-derived growth factor B (PDGFB) in glial progenitor cells), by reducing the M2 polarization and increasing the phagocytosis of TAMs.[46] Evidences also showed that the tumor infiltration process of CD8+ T cells was increased and the tumor growth rates in both mammary and cervical tumor model were attenuated after inhibiting CSF-1/CSF-R pathway with BLZ945.[26] However, BLZ945 has poor solubility in water (<1 mg/mL). Despite the low IC50 value (1 nM) for BLZ945, large quantities of the BLZ945 (~ 200 mg/kg) were dosed orally daily to achieve the

therapeutic effect of this drug on the gliomas in PDG mice.[46] We hypothesized that by conjugating BLZ945 drug to the dendrimer through a pH and esterase sensitive linker, we could improve the solubility, targeting capability and bioavailability of BLZ945.

Compound/Class	Target	Clinical Phase	Sponsor	Tumor type
PLX3397 / small molecule	CSF1R (and cKit, Fit3)	II/III	Plexxikon/Daiichi Sankyo Inc.	Solid tumors, Glioblastoma, Hodgkin lymphoma, Malignant melanoma, PVNS
ARRY-382 / small molecule	CSF1R	I	Array Biopharma	Solid tumors
FPA008 / mAB	CSF1R	Ia/Ib	FivePrime/BMS	Solid tumors
IMC-CS4 (LY3022855) / mAB	CSF1R	I	Eli Lilly	Solid tumors
JNJ-40346527 / small molecule	CSF1R	I	Johnson & Johnson	Hodgkin lymphoma

Table 1 Therapeutic agents targeting CSF1R in clinical trials. (mAB: monoantibody). [44]

EC_{50}	PLX3397	JNJ-40346527	ARRY-382	BLZ945
CSF1R(c-fms)	20 nM	0.69 nM	9 nM	1 nM
cKit	10 nM	5 nM	nd	3880 nM
PDGFRb	nd	nd	nd	5860 nM
PDGFRa	nd	nd	nd	>10000 nM
FIt3	160 nM	30 nM	nd	>10000 nM
LCK	860 nM	88 nM	nd	>10000 nM
VEGFR2(KDR)	350 nM	nd	nd	>10000 nM

Table 2 Selectivity of small molecule to kinase. (nd=not disclosed). [45]

2.2 Materials and methods

2.2.1 Materials

Hydroxyl- polyamidoamine (PAMAM) dendrimer (64 G4-OH end groups) was obtained from Dendritech (Midland, MI, USA). BLZ945 was obtained from ChemShutle (Hayward, CA). PD98059 was purchased from selleckchem (Houston, TX). Succinic anhydride, glutaric

anhydride, Oxydiethylene bis(chloroformate), Methyl-4-chloro-4-oxobutanoate, 5-bromo pentanoic acid, triethylamine (TEA), dichloromethane (DCM), dimethyl formamide (DMF), N,N'-diisopropylethylamine (DIEA) were obtained from Sigma-Aldrich (St. Louis, MO, USA) in highest quality available. 3-(2-Pyridyldithio)propanoic Acid was obtained from Toronto Research Chemicals (Toronto, Canada). (Benzotriazol-1-yloxy)tripyrrolidino-phosphonium hexafluorophosphate (PyBOP), DMAP and DCC were obtained from Bachem Americas Inc. (Torrance, CA,USA). Silica gel GF254 plates for Thin-layer chromatography (TLC) were purchased from Whatman (Piscataway, NJ). Proton NMR spectra were obtained using Bruker (500 MHz) spectrometer with DMSO-d6 solvent from Cambridge Isotope Laboratories, Inc. (Andover, MA). Proton chemical shifts were reported in ppm (d) and tetramethylsilane (TMS) was used as internal standard.

2.2.2 Synthesis of D-PD98059 conjugate

(1) Synthesis of PD98059 linker

To generate the proper linker between PD98059 and PAMAM dendrimer, we tried different strategies to activate the aromatic amine functional handle.

Reaction A:

To the solution of PD98059 (25 mg, 0.0935 mmole) in DMF (10 mL), sodium hydride (2.24 mg, 0.0935 mmole) was added and stirred for 5 min under nitrogen atmosphere, to this mixture 5-bromo pentanoic acid (18.6 mg, 0.1028 mmole) was added and stirred at room temperature for 24 h (**Scheme 1**). Adding isopropanol drop by drop at cold condition quenched the reaction mixture and then concentrating the reaction mixture via rotary evaporation. To this residue ethylacetate and water is added to extract organic components in ethylacetate. To this organic fraction sodium sulfate was added to remove any residual water

fraction and supernatants were collected and concentrated by rotary evaporation. All the organic compounds from this method were separated via column chromatography and analyzed by NMR, according to NMR analysis, the intended product did not form this is attributed to poor reactivity of PD98059 aromatic amine.

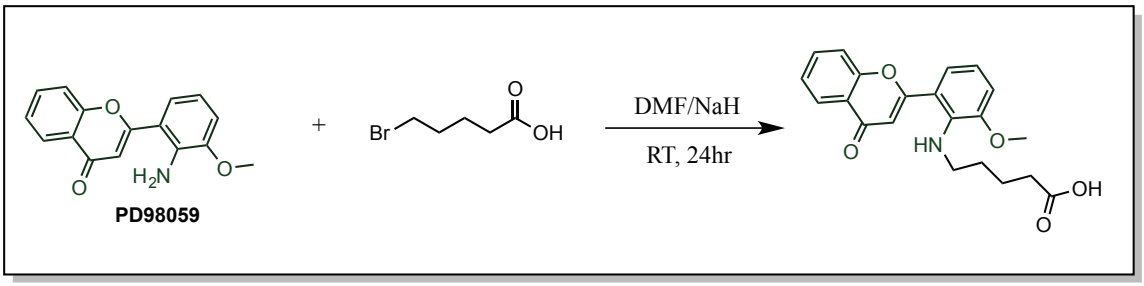

Scheme 1. Preparation of PD98059 carboxylate linker

Reaction B:

To the solution of PD98059 (25 mg, 0.0936 mmole) in dry THF at 0°C, add triethylamine and stir for 10 minutes under nitrogen atmosphere. Then add glutaric anhydride (10 mg, 0.0936 mmole) dissolved in dry THF and stir for overnight, no product formation is observed according to TLC (**Scheme 2**).

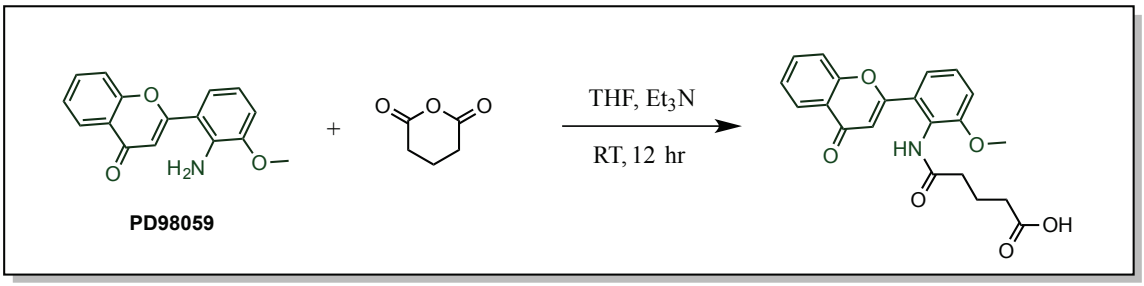

Scheme 2. Preparation of PD98059 glutarate linker

Reaction C:

To the solution of PD98059 (25 mg, 0.0936 mmole) in dry THF at 0°C, added triethylamine and stirred for 10 minutes under nitrogen atmosphere. Then add succinic anhydride (10 mg,

0.0936 mmole) dissolved in dry THF and stir for overnight, no product formation is observed according to TLC (**Scheme 3**).

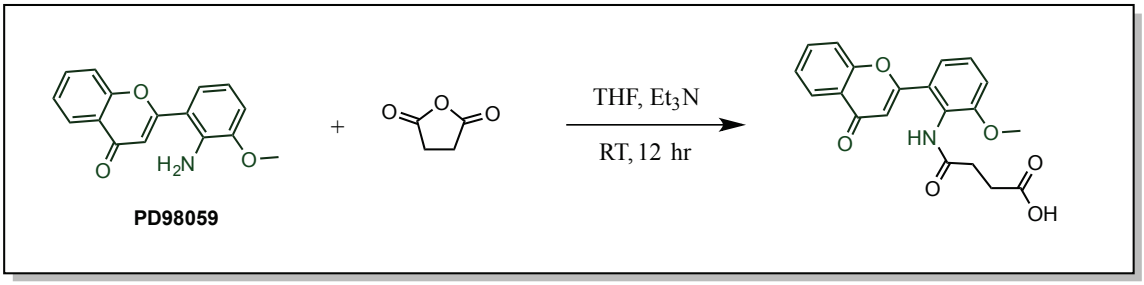

Scheme 3. Preparation of PD98059 succinate linker

Reaction D:

PD98059 (10 mg, 0.0374 mmole) was dissolved in 10mL DCM and added triethylamine. Stirred for 10 minutes under nitrogen atmosphere. Then Methyl-4-chloro-4-oxobutanoate (10 uL, 0.0748 mmole) was added into the DCM solution (**Scheme 4**). After 18 h, TLC showed no product formation. Thus we added half of original volume of Methyl-4-chloro-4-oxobutanoate and triethylamine to the reaction and let it go for another 24 h. There was still no product formation.

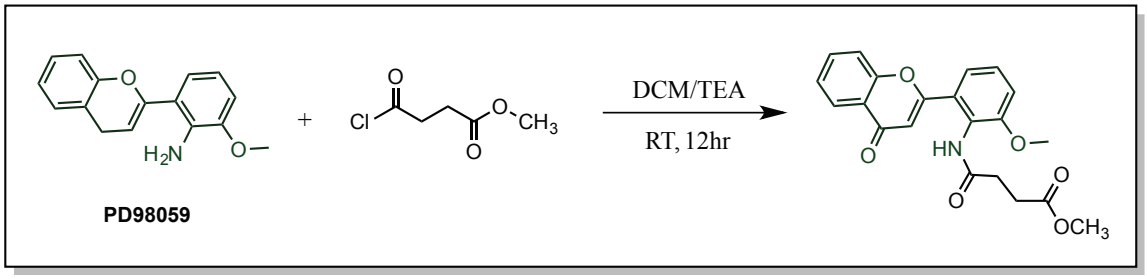

Scheme 4. Preparation of PD98059 methoxy ester linker

Reaction E:

To the solution of PD98059 (25 mg, 0.0935 mmole) in DCM at 0 °C DCC/DMAP were added and stirred for 10 min then 3-(pyridin-2-yl disulfanyl)propanoic acid (45mg, 0.186

mmole) was added slowly over a period of 5 min. The resulting reaction mixture was stirred for 24 h (**Scheme 5**). According to TLC no product formation was observed.

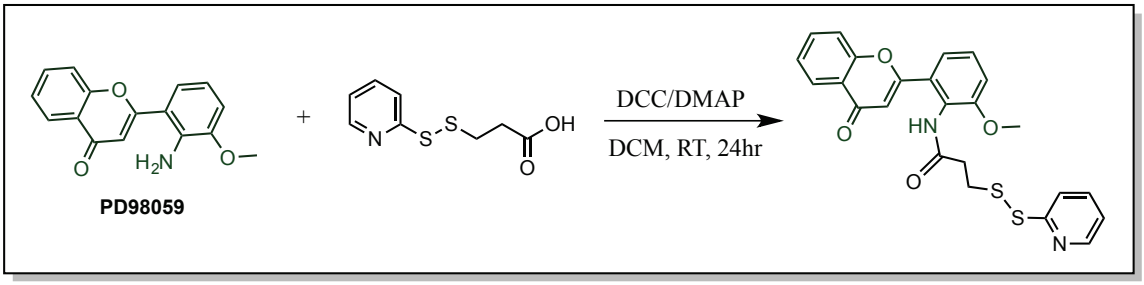

Scheme 5. Preparation of PD98059 pyridyl disulfide linker

Reaction F:

PD98059 (30 mg, 0.112 mmole) was dissolved in 10mL DCM and stired under nitrogen, 0°C for 10 minutes. Then ethylene-bis-choloroformate (200 uL, 1.122 mmole) was added drop by drop into the DCM solution. The reaction was done at 0°C for 24 h (**Scheme 6**). According to thin layer chromatography (TLC) all the starting material is consumed at this stage, we added silica gel (500 mg) to make slurry and performed column chromatography with ethyl acetate and hexanes to extract pure compound, PD98059 linker (yield 90%, 70.3mg).

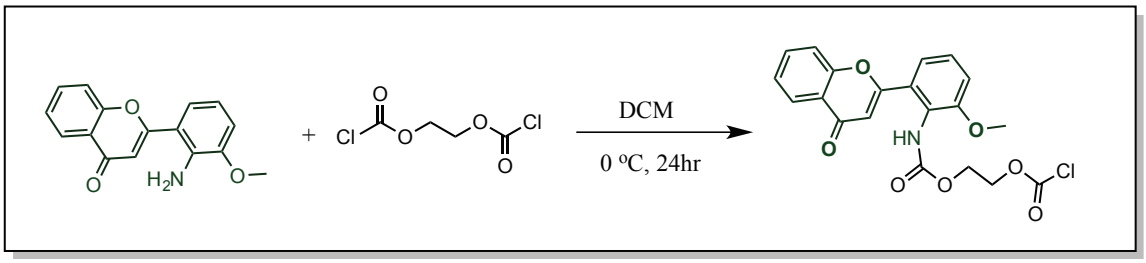

Scheme 6. Preparation of PD98059 chloroformate linker

Among all the reactions for PD98059 linkers, PD98059 was consumed completely only in reaction F (**Scheme 6**) with ethylene-bis-chloroformate. In reactions A, B, C and D, there were significant amounts of reactant PD98059 left even after reacting for 48 h. The PD98059

urethane linker from reaction F was then treated with G4OH dendrimer to form the dendrimer-PD98059 conjugate.

(2) Synthesis of dendrimer-PD conjugate

To the solution of PD98059 urethane linker **(3, Figure 4)** (30 mg, 0.072 mmol) in DMF (15 mL), added DIEA (38 uL, 0.215 mmol). Stirred under nitrogen atmosphere in an ice bath for 20 minutes. Then hydroxyl PAMAM Dendrimer G4OH **(4)** (180 mg, 0.012 mmol) was added into the mixture and stirred for 48 h (**Figure 4**). Silica gel was added into the flask to make slurry and column chromatography was performed with 3-5% Methanol in DCM to extract the pure compound D-PD98059 **(5)**. After evaporated and re-dissolved the extracted portion, dialysis was performed in DMF (membrane MW cutoff = 2 kDa) for 48 h and the solvent was changed for 5 times. The obtained solution was evaporated under reduced pressure at room temperature, followed by high vacuum overnight, to obtain an semi-solid D-PD98059 conjugates. The semi-solid conjugates were dissolved in DI water (0 ˚C) and dialyzed in DI water (membrane MW cutoff = 2 kDa) at 4 °C for 5 h, where changed the water every hour to get rid of DMF. The resultant water layer was lyophilized to get the powder of pure D-PD98059 **(5)**. The D-PD98059 **(5)** conjugates were characterized by ^{1}H-NMR (**Figure 5**).

2.2.3 Synthesis of D-BLZ945 conjugate

(1) Synthesis of BLZ945-succinate linker

BLZ945 **(6)** (100 mg, 0.25 mmol) was dissolved in DCM (25 mL) in 100 mL round bottomed flask under nitrogen atmosphere, to which triethylamine (210 uL, 1.5 mmol) was added. Stirred for 10 minutes and added succinic anhydride **(7)** (250 mg) that had dissolved in DCM (**Scheme 8**). Let the reaction go for 24 h and check TLC. The TLC results showed

there were BLZ945 left in the system, and thus half of original amount of succinic anhydride and triethylamine were added to the reaction. After 8 h, all the starting material (BLZ945) was consumed at this stage according to TLC. We then added silica gel to make slurry and performed column chromatography with ~5% Methanol in DCM to extract pure compound, BLZ945-succinate linker **(8)** (120 mg, yield 95%). The BlZ945-succinate linker was characterized by ^{1}H-NMR (A**, Figure 7**).

(2) Synthesis of D-BLZ945 conjugate

To the solution of BLZ945-succinate linker (120 mg, 0.24 mmol) in DMF (20 mL), added PyBOP (224.8 mg, 0.432 mmol) and DIEA (75uL, 0.432 mmol). The solution was stirred under nitrogen atmosphere in an ice bath for 20 minutes. Then hydroxyl PAMAM Dendrimer G4OH **(4)** (336 mg, 0.024 mmol) was added into the mixture and stirred for 48 h. Silica gel was added into the flask to make slurry and column chromatography was performed with 3-5% Methanol in DCM to extract the pure compound D-BLZ945 **(9).** After evaporated and re-dissolved the extracted portion, dialysis was performed in DMF (membrane MW cutoff = 2 kDa) for 48 h and the solvent was changed for 5 times. The obtained solution was evaporated under reduced pressure at room temperature, followed by high vacuum overnight, to obtain an orange semi-solid D-BLZ945 conjugates. The semi-solid conjugates were dissolved in DI water (0 ˚C) and dialyzed in DI water (membrane MW cutoff = 2 kDa) at 4 °C for 5 h, where changed the water every hour to get rid of DMF. The resultant water layer was lyophilized to get fluffy light yellow powder of pure D-BLZ945 **(9)**. The structure of D-BlZ945 conjugate was characterized by ^{1}H NMR (B**, Figure 7**).

2.2.4 High performance liquid chromatography (HPLC) characterization of the conjugates

The purity of the D-BLZ945 conjugates was analyzed using HPLC (Waters Corporation, Milford, MA) with a 1525 binary pump, 2998 photodiode array (PDA) detector, 2475 multiwavelength fluorescence detector and 717 auto sampler interfaced with Empower software. The HPLC chromatograms were monitored at 254 nm using PDA detector. The mobile phase was water/acetonitrile (0.1% w/w TFA). The column used for this study was symmetry c18 column, 300 A, 5 μM, 4.6 mm X 250 column with corresponding guard column. A gradient flow was used with the initial condition of 90:10 (Water/ACN) was maintained until 10 minutes and gradually changing to the ratio to 10:90 (Water/ACN) until 30 min and then back to 90:10 for 20 min with flow rate of 1 mL/min for all conjugates.

2.2.5 Dynamic light scattering (DLS) and zeta potential (ζ)

The particle size and ζ-potential of D-BLZ945 conjugates were measured by dynamic light scattering (DLS) using a Zetasizer Nano ZS (Malvern Instrument Ltd. Worchester, UK) with a 50 mW HeNe laser (633 nm). The D-BLZ945 conjugates were dissolved in deionized water to make the solution with the final concentration of 0.1 mg/mL. The solution was filtered through a cellulose acetate membrane (0.45 μm, PALL Life Sciences) and DLS measurements were performed in triplicate, at 25 °C with a scattering angle of 173°.

2.2.6 Drug release study

The release of BLZ945 from the D-BLZ945 conjugates was determined in PBS (pH 7.4), Citrate buffer (pH 5.5). We chose these two buffers to simulate the extracellular condition (pH 7.4) and lysosomes (pH 5.5). A concentration of 3 mg/mL was maintained at 37 ˚C in a

shaker. 600 µL solution was collected from the incubation mixture and frozen at -80 ˚C till the final analysis. The percent of released BLZ945 from DBLZ945 was quantified using HPLC (**Figure 10**).

2.3 Results and discussion

2.3.1 Synthesis of dendrimer-PD98059 (D-PD98059, 5)

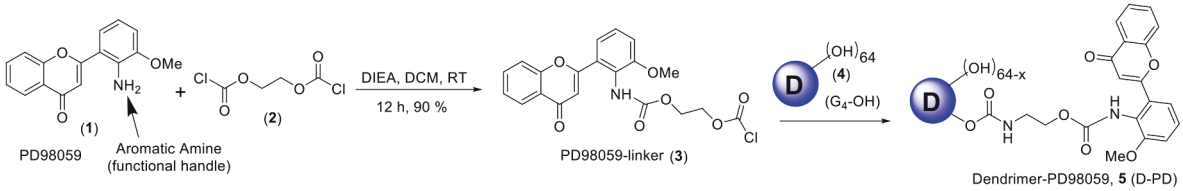

Figure 4 Schematic representation of PD98059 urethane linker, **3** and D-PD98059 conjugate preparation.

The drug molecule, PD98059 **(1)**, has one aromatic amine functional handle; we attempted to functionalize this amine with carboxylic acid linkers (such as 4-hydroxy butanoic acid) to form corresponding amides, via multiple coupling chemistries (EDC/DMAP, DCC/DMAP and PyBOP/DIEA) and also by treating PD98059 with reactive acid chlorides to form amides with no success. Then, we switched our strategies (Figure 4) to make a PD98059 urethane linker **(3)** by treating PD98059 with Ethylene-bis-chloroformate **(2)**. Following this strategy, we made PD98059 urethane linker **(3)** with reactive chloroformate, which upon treatment with hydroxyl terminal PAMAM dendrimer forms a dendrimer-PD98059 conjugate (D-PD98059, **5**). The characteristic peaks at 7.50 ppm and 8.0 ppm regions corresponded to D-PD98059 (**Figure 5**). Unfortunately, this conjugate did not release PD98059 in various aqueous solutions (in the pH range of 2-12) or buffer conditions.

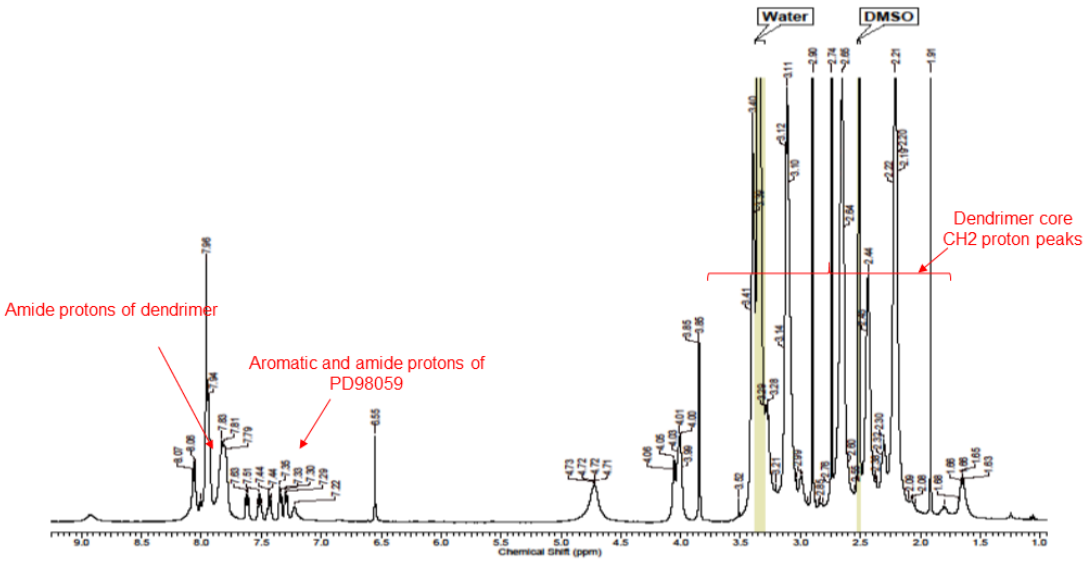

Figure 5 ^{1}H-NMR data for D-PD98059 conjugates

2.3.2 Synthesis of dendrimer-BLZ945 conjugate (D-BLZ945, 9)

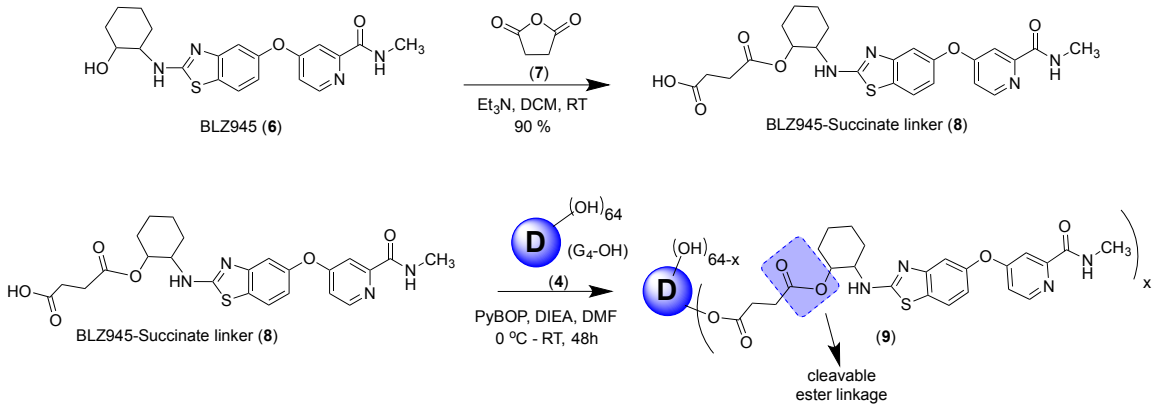

Figure 6 Schematic representation of BLZ945 succinate linker, **8**, and esterase cleavable D-BLZ945 conjugate, **9**, preparation.

BLZ945 has primary hydroxyl functional group that acts as a good functional handle to form D-BLZ945 conjugates. The esterase cleavable D-BLZ945 (**9**) was obtained by conjugation of

BLZ945 **(6)** with succinate linker **(7)** to G4OH dendrimer **(4)** using a two-step synthesis strategy. BLZ945 (**6**) drug was treated with succinic anhydride (**7**) resulting in the formation of BLZ945-succinate linker (**8**). This compound **8** was treated with generation four hydroxyl terminal PAMAM dendrimer (**4**) to form pH and esterase sensitive D-BLZ945 conjugate (**9, Figure 6**). The conjugate **9** was extensively purified by dialysis and chromatographic techniques and its structure was confirmed by complementary techniques such as ^{1}H-NMR, ^{13}C-NMR, HPLC, and MALDI analysis. From BLZ945 linker ^{1}H-NMR (B, **Figure 7**), the characteristic peaks at 12.13 ppm region indicated the carboxylate linker formation and this was further supported by the presence of CH_2 protons of succinate linker at 2.3 ppm. Similarly, D-BLZ945 conjugate formation was confirmed by the presence of amide protons of dendrimer at 7.96 ppm (C, **Figure 7**). According to NMR analysis, there was approximately 20% (w/w) drug loading per dendrimer.

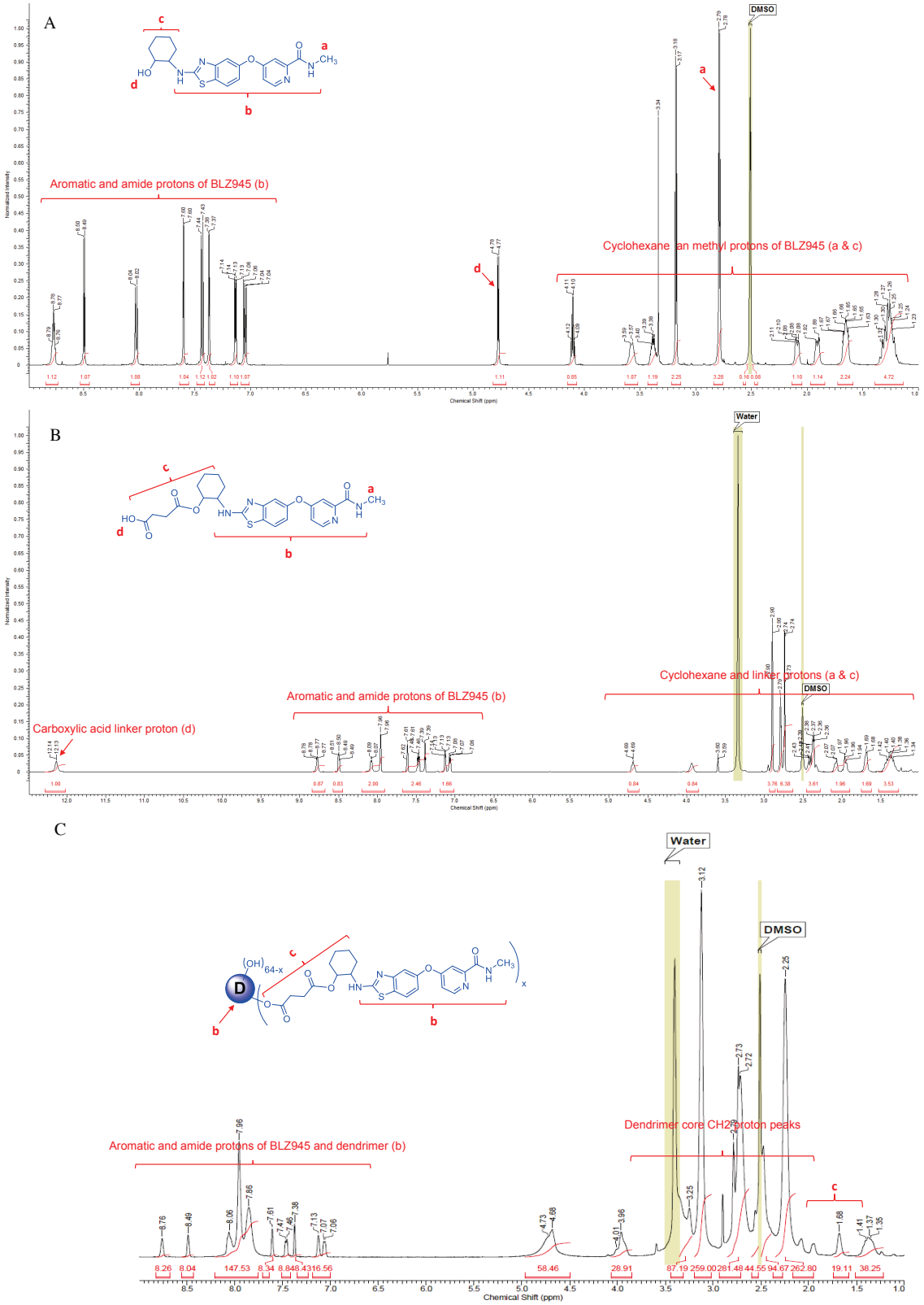

Figure 7 ^{1}H-NMR spectra of (A) BLZ945, (B) BLZ945-succinate linker and (C) G4OH D-BLZ945 conjugates.

2.3.3 HPLC characterization of D-BLZ945 conjugates

D-BLZ945 conjugate, BLZ945-Succinate linker and BLZ945 were separated at least 3 minutes using HPLC method. The purity of D-BLZ945 and BLZ945-Succinate linker were determined using reverse phase HPLC. A gradient flow was used with the initial condition of 90:10 (Water/ACN) was maintained until 10 minutes and gradually changing to the ratio to 10:90 (Water/ACN) until 30 min and then back to 90:10 for 20 min with flow rate of 1 mL/min for all conjugates. The HPLC data showed that free BLZ945 eluted at 16.7 min, BLZ945-Succinate linker eluted at 20.2 min and D-BLZ945 eluted at 49.4 min as a broad peak observed at 254 nm absorption (**Figure 8**). The broad peak of D-BLZ945 was a result of the molecular weight distribution of the conjugates, mainly from the different numbers of BLZ945 linked to each dendrimer.

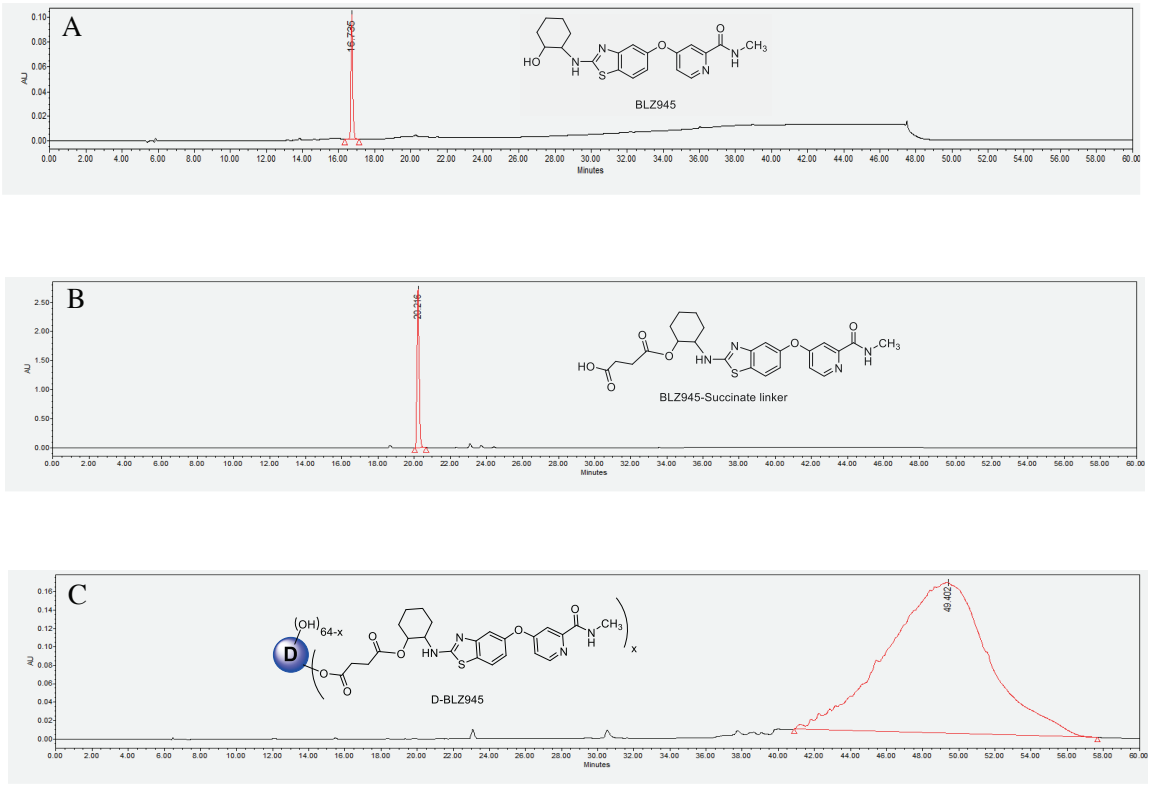

Figure 8 HPLC chromatograms of BLZ945 (16.735 min), BLZ945-succinate linker (20.216 min) and D-BLZ945 (49.402 min) monitored at 254 nm.

2.3.4 D-BLZ945 conjugate is small nanoparticle with positive surface charge.

The size and zeta potential of D-BLZ945 conjugate was investigated. We synthesized two batches of D-BLZ945 in total. The size of D-BLZ945 was around 5.4 nm in the D-BLZ945 conjugate with Mw of 16,200 and around 7.0 nm for D-BLZ945 with Mw of 19200. The zeta potential was (**2.5 ± 0.1 mV**) for the D-BLZ945 conjugates with Mw of 16,200 and (**3.1 ± 0.3 mV**) for conjugates with Mw of 19,200 (**Figure 9**). The solubility of D-BLZ945 with Mw of 19200 was 10 mg/mL in water, which was much higher than BLZ945 (almost insoluble in water).

Batch	Mw	% loading of BLZ945	# of BLZ945 molecules	Diameter (nm)	ζ-potential
1	**~16,200**	**8-10 %**	**~ 4**	**~5.4**	**2.5 ± 0.1 mV**
2	**~19,200**	**18 – 20 %**	**~ 10**	**~7.0**	**3.1 ± 0.3 mV**

Figure 9 Characterization of synthesized D-BLZ945 conjugates

2.3.5 D-BLZ945 conjugates release free BLZ945 rapidly.

We studied the release of drug from the conjugate by monitoring the release by HPLC technique. The release rate of BLZ945 from D-BLZ945 conjugates was investigated in PBS (pH 7.4) and citrate buffer (pH 5.5) to simulate the extracellular and lysosomes pH respectively. Calibration curves for BLZ945, BLZ945-Succinate linker and D-BLZ945 were established over a concentration of 1 ng to 1 mg at 254 nm, the limit of detection for the molecule was found to be at 10 ng. HPLC method was used to quantify the released BLZ945 and BLZ945 linker and D-BLZ945 conjugate.

According to the HPLC results (**Figure 10**), over 80% BLZ945 released in 5 days at pH = 5.0 and in 8 days at pH = 7.4, and the drug predominately released as free BLZ945. These drug release rates of D-BLZ945 were acceptable for delivering BLZ945 to TAMs in glioblastoma. Previous research showed that G4OH dendrimers were able to accumulated in the brain tumor from 15 min to 48 h upon systemic injection in a 9L gliosarcoma tumor model.[10] Thus the rate that over 40% BLZ945 were released in 24 h at pH=5.0 would be sufficient for D-BLZ945 to exhibit the therapeutic efficacy of BLZ945 at the tumor site within 48 h. In current research of BLZ945, oral dose of 200 mg per kg body weight was used daily to achieve therapeutic effect.[46] Considering the targeting ability of G4OH dendrimer, D-BLZ945 with these drug release rates would be able to potentially improve the bioavailability of BLZ945 with lower dose and less frequency.

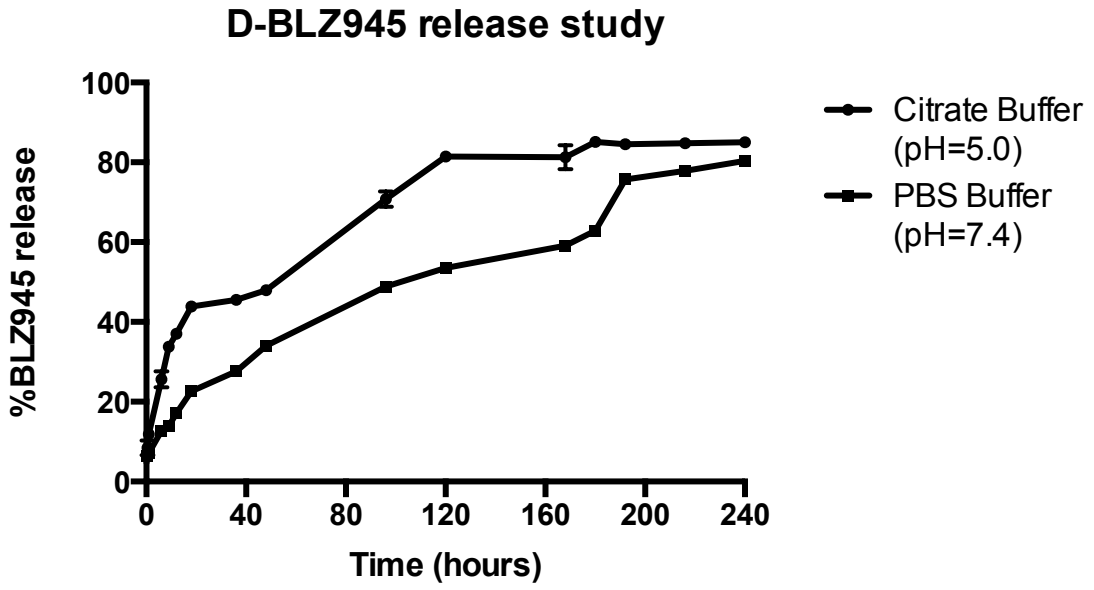

Figure 10 In vitro drug release rate of D-BLZ945 in PBS buffer (pH 7.4) and Citrate Buffer (pH 5.0).

2.4 Summary

We developed D-PD98059 conjugates with urethane linker and D-BLZ945 conjugates with succinate linker. We tried multiple strategies to functionalize the aromatic amine in PD98059 with carboxylic acid linkers with no success and turned to the strategy of making a PD98059 urethane linker. However, this D-PD98059 conjugate with urethane linker lack drug release up to 20 days. By contrast, D-BLZ945 conjugates with succinate linker have a release rate of free BLZ945 by over 90% within 10 days. D-BLZ945 conjugates have approximate 20% (w/w) drug loading and exhibit enhanced water solubility compared to free drug. The efficacy of D-BLZ945 was evaluated and shown in chapter 3.

Chapter 3: *In vitro* evaluation of the therapeutic efficacy of D-BLZ945 and D-PD98059 conjugates.

3.1 Introduction

Tumor associate macrophages (TAMs) play key roles in establishing the microenvironment for tumor growth and migration.[47,48] Different phenotypes of macrophage are activated by distinct stimulating signals from T cells or tumor cells at different stages of tumor growth.[19] Many therapeutic methods have been explored to control tumor growth by targeting and modulating TAMs in malignant tumors like breast cancer and liver cancer.[49,50,51] In response to the stimulations, polarized macrophages express cytokines to either promote inflammation or inhibit immune activity against carcinoma. Pro-inflammatory M1 type of macrophages is dominant at early stage of tumor initiation, generating cytokines and growth factors that help create chronic inflammation.[52] Chronic inflammation is considered as a potential cause of

multiple cancers. M2 macrophages become dominant upon the establishment of tumor and create an anti-inflammatory environment to promote tumor growth.[16] LPS, IFN-γ and TNF-α polarize macrophages to be M1 subtype, which is featured by high expression level of cytokines like IL1β, IL12 and TNF-α. On the other hand, IL4, TGFβ, IL10 and CSF1 could polarize macrophages to be M2 subtype, which is featured by high IL-10 expression, low IL-12 expression and higher of arginase-1 production in cell.[17, 19]

BLZ945, the CSF1R inhibitor, has shown to block the CSF1/CSF1R messaging between tumor cells and macrophages, which decreased M2 marker expression and hindered tumor growth.[46] PD98059, the specific inhibitor for MAPK kinase, has the potential to inactivate MAPK pathway in M1 macrophages and inhibits pro-inflammatory response.[30,41, 53] D-BLZ945 and D-PD98059 have greater solubility than free drug and one dendrimer carry several free drugs that would increase the effective concentration in the targeting sites. We envision the better targeting ability, efficacy and biovialiability of the dendrimer conjugates.

By investigating at the protein level of Arg-1 and the RNA level of pro-inflammatory cytokines (IL1β, IL6 and TNFα), I evaluated the potential therapeutic effect of D-BLZ945 and D-PD98059 respectively and compared them to free drugs. The cytotoxicity of dendrimer conjugates and free drugs were also studied in this chapter.

3.2 Materials and Method

3.2.1 Cell culture for microglia and macrophage cells

The BV2 mouse microglia cell line was from Children's Hospital of Michigan Cell Culture Facility, and the Raw264.7 macrophage cell line was purchased from ATCC. Both of the cells were cultured in Dulbecco's modified Eagle's medium (DMEM, Life technologies)

with 5 % fetal bovine serum (FBS, Invitrogen) and 1% penicillin-streptomycin (P/S, Invitrogen) at 37 ˚C with 5% CO2 in an incubator.

3.2.2 Preparation of BLZ945 and D-BLZ945 formulations for in vitro study

BLZ945 was dissolve in DMSO to make a 1 mg/mL solution and D-BLZ945 (10% drug payload) was dissolved in medium containing 10% DMSO to make a 1 mg/mL solution. These solutions were diluted to the different concentrations with fresh DMEM medium. The conjugate concentrations were showed in terms of corresponding free drug concentrations in it. All the solutions were prepared freshly right before treatment.

3.2.3 Preparation of PD98059 and D-PD98059 formulations for in vitro study

PD98059 was dissolved in DMSO to make a 2 mg/mL solution and then diluted with media to different concentrations. D-PD98059 was dissolved in medium containing DMSO with same percentage as drug payload of the conjugate and diluted with fresh medium. The conjugate concentrations were showed in terms of corresponding free drug concentrations in it.

3.2.4 Cytotoxicity studies

BV2 cells were seeded in 96 well plates (Costar) with a concentration of 10,000 cells/well (100 μL/well) and incubated for 24 h. Then the cells were treated with culture medium containing different concentrations (10^{-9} to 10^{-5} g/mL) of BLZ945 and D-BLZ945 at increasing concentrations for 24 h. Cell viability was evaluated using alarmaBlue kit (Invitrogen). Absorbance at 600 nm and 570 nm were read using fluorescence microplate reader (BioTek Instruments). The cell viability was calculated using the equations given in the kit and normalized as percentage relative to control group.

The cytotoxicity of BLZ945 and D-BLZ945 on IL4 treated BV-2 and Raw264.7 cells were also measured. At 24 h after seeding (96 well plates, 10,000 cell/w seeding density), the cells were treated with fresh media containing experimental concentrations of BLZ945 and D-BLZ945 (2, 20, 200 ng/mL) 1 h before adding IL4 (10 ng/mL) for 24 h co-treatment. Cell viability was measured in the same method described above.

3.2.5 Western blot to analyze CSF1R activation and Arg1 expression levels

BV2 cells were plated in 6 well plates with seeding density of 300,000 cells/well and cultured with phenol red free DMEM (10% FBS, 1% P/S). The cells treated with BLZ945, D-BLZ945 (2, 20 and 200 ng/mL) and DMSO as a control group for 2 h before adding IL4 for 24 h co-treatment. For evaluating CSF1R activation, BV2 cells were treated with BLZ945 or D-BLZ945 (20, 200 and 2000 ng/mL) 12 h before changing fresh media and stimulating with CSF1 for 30 min.

The protein samples were harvested with 150 μL T-per buffer (ThermoFisher Scientific) containing Pierce EDTA-Free protease inhibitor (ThermoFisher Scientific) and sodium orthovanadate (Santa Cruz) as phosphatase inhibitor. Protein concentrations were determined using Pierce™ BCA Protein Assay Kit (ThermoFisher Scientific). The proteins were separated on 10% SDS-PAGE gels (Biorad) at 120 V for about 1 hour and transferred to polyvinylidene fluoride membrane (PALL) at 80 V for 1 hour. The membranes were blocked with 5% w/v Bovine serum albumin (BSA) solution (Sigma-Aldrich) for 1 hour at room temperature. After primary antibody incubation on a rocker in cold room (4 ˚C) overnight, the membranes were placed in corresponding horseradish peroxidase (HRP) conjugated secondary antibody for 1 hour at room temperature. The protein bands were visualized using enhanced chemiluminescence (ECL) western blotting substrate (Promega Corporation) and

HyBlot CL autoradiography film (Denville Scientific Inc.). Quantitative densitometric analysis was performed using Multi Gauge software (Fujifilm).

The following primary antibodies were used: Arginase-1 antibody (1:1000, #9819, Cell Signaling); phosphor-M-CSF Receptor (Tyr723) (49C10) antibody (1:1000, #3155 Cell Signaling); M-CSF Receptor antibody (1:1000, #3152, Cell Signaling); phosphor-Akt (Ser473) Antibody (1:1000, #9271, Cell Signaling); Akt (pan) (C67E7) antibody (1:1000, #4691, Cell Signaling) and β-actin (1:10,000, A5316, Sigma-Aldrich).

3.2.6 RT-qPCR to analyze pro-inflammatory cytokine RNA levels

BV2 cells were treated with LPS for 3 h, followed by free PD, D-PD and free dendrimer treatment with different doses for 6 and 24 h. Total RNA from cells was extracted using TriZol and 1ug RNA was reverse-transcribed into cDNA using High Capacity RNA-to cDNA kit (Applied Biosystems). The temperature profile was as follows: 37°C for 1 hour, 95°C for 5 minutes and then 4°C for 1 hour. Then PCR amplification was quantified with Fast SYBR® Green Master Mix kit (Applied Biosystems).

3.3 Results and Discussion

3.3.1 *In vitro* efficacy of D-BLZ945

(1) Cytotoxicity of D-BLZ945 and BLZ945 on microglia and macrophage

A cytotoxicity study was performed in BV2 microglia cells for D-BLZ945 conjugates and BLZ945 (**Figure 11**). BLZ945 is known as a highly potent inhibitor for CSF1R with 1 nM IC_{50} and 67 nM EC_{50} for bone marrow-derived macrophages (BMDMs).[46] Thus 1 ng/mL was chosen as the lowest concentration and 10 μg/mL was chosen as the highest concentration which already contains 1% DMSO. BV2 cells were treated with BLZ945 and D-BLZ945 in a

concentration range from 0.001 to 10 μg/mL for 24 h. The concentration of D-BLZ945 was shown in terms of equivalent concentrations of BLZ945. AlarmaBlue assay showed that D-BLZ945 and BLZ945 didn't show significant toxicity on BV2 cells cells up to 10 μg/mL after 24 h treatment (**Figure 11).** Because I was interested in investigating the effect of D-BLZ945 on M2 subtype, the toxicities of D-BLZ945 and BLZ945 on IL4 activated microglia cells were also evaluated (**Figure 12**) to make sure the potential inhibitory efficacies in the following experiments are not from cell death. The concentrations of 2 ng/mL (5 nM), 20 ng/mL (50 nM) and 200 ng/mL (500 nM) were chosen for this purpose. The results showed that D-BLZ945 and BLZ945 didn't have significant toxicity to IL4 activated BV2 microglia cells after 24 h. D-BLZ945 exhibited higher cell viability in the highest concentration group (200 ng/mL) than BLZ945.

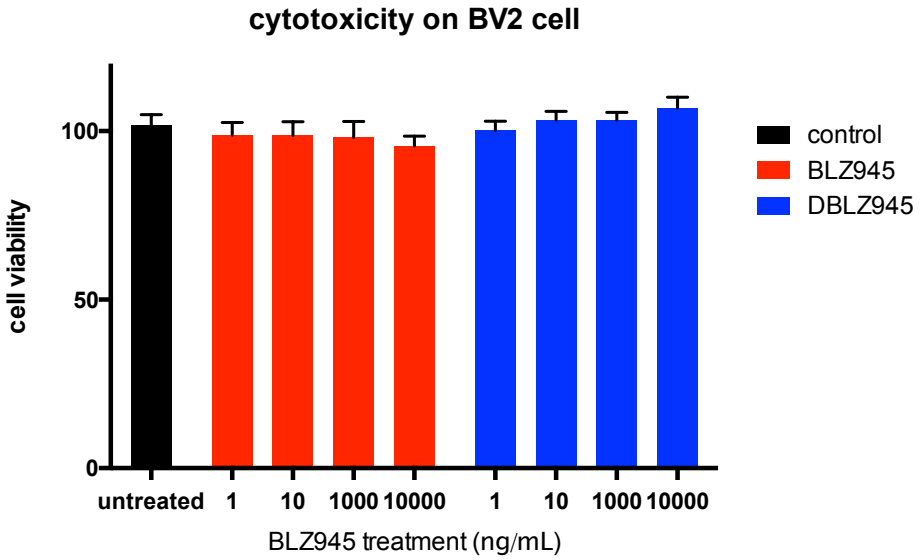

Figure 11 Cytotoxicity of BLZ945 and D-BLZ945 on BV2 microglia cells. BV2 cells (P: 19) were treated with BLZ945 and D-BLZ945 (0.001, 0.01, 1 and 10 μg/mL) for 24 h. Cell viability was measured using alarmaBlue assay. n=6 independent replicates.

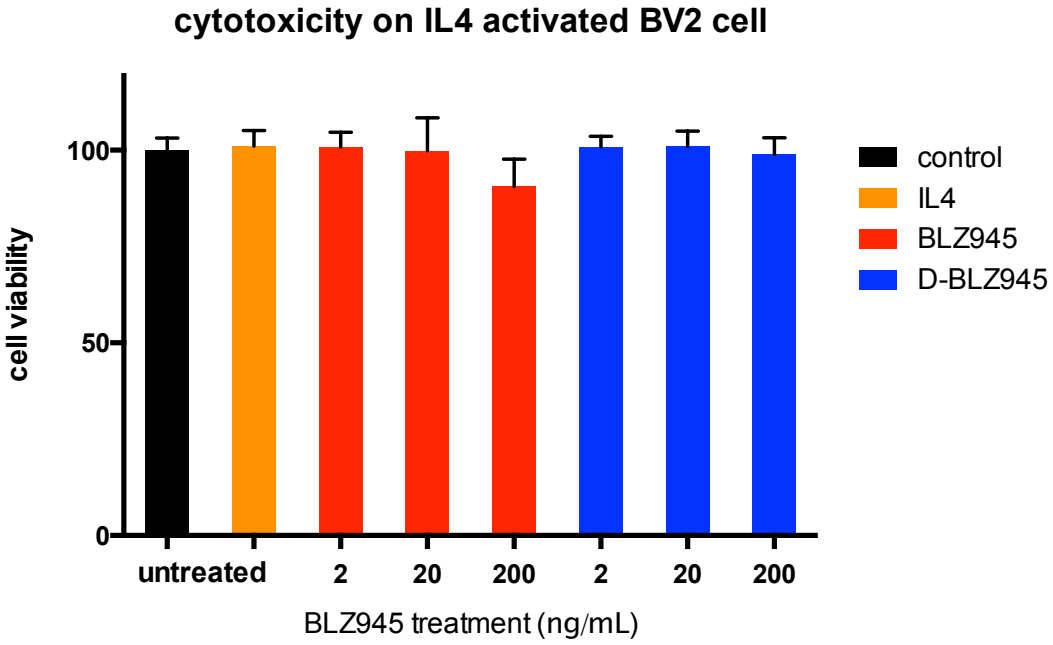

Figure 12 Cytotoxicity study of BLZ945 and D-BLZ945 on IL4 activated BV2 microglia cells. BV2 cells (P22) were treated with BLZ945 and D-BLZ945 (2, 20 and 200 ng/mL) one hour before adding IL4 for 24 h co-incubation. Cell viabilities were measured using alarmaBlue assay. n=6 independent replicates.

By comparison, we measured the toxicity of D-BLZ945 and BLZ945 on another macrophage cell line Raw264.7 with IL4 stimulation (**Figure 13**). No significant toxicity was observed after 24 h for both BLZ945 and D-BLZ945.

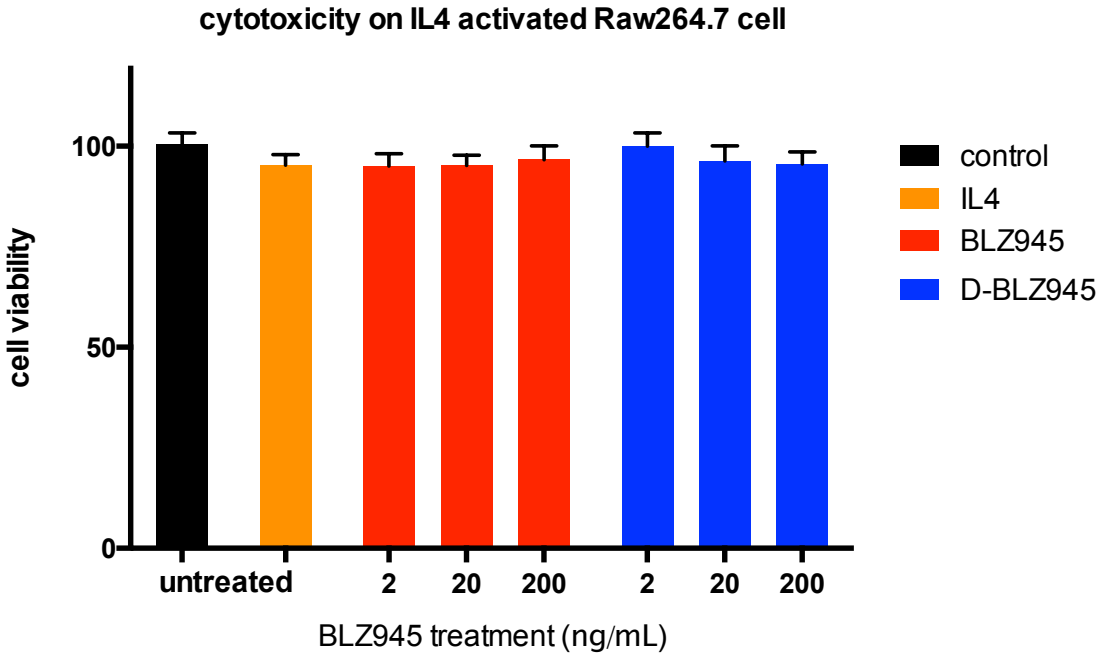

Figure 13 Cytotoxicity study of BLZ945 and D-BLZ945 on IL4 activated Raw264.7 macrophages. Raw264.7 macrophage cells (P: 3) were treated with BLZ945 and D-BLZ945 (2, 20 and 200 ng/mL) one hour before adding IL4 for 24 h co-incubation. Cell viability was measured using alarmaBlue assay. n=6 independent replicates.

(2) Inhibitory effect of D-BLZ945 and BLZ945 on CSF1R phosphorylation

BLZ945 is a potent CSF1R inhibitor with IC_{50} of 1 nM in a cell free assay.[46] To evaluate the inhibitory effect of D-BLZ945 and BLZ945 on CSF1R, protein level of CSF1R activated form (phosphor-CSF1R) was measured after drug treatment on BV2 microglia cells (**Figure 14**). The upper row was the western blot results and the lower row was the quantification of the upper graph by normalizing them to the control with arbitrary units. BV2 cells were treated with BLZ945 or D-BLZ945 for 12 h prior to 30 min stimulation with CSF1 (A, **Figure 14**). Up-regulated phosphor-CSF1R expression was observed following CSF-1 stimulation, and it was effectively inhibited by D-BLZ945 and BLZ945. BLZ945 exhibited inhibitory effect on CSF1R phosphorylation at 20 ng/mL (50 nM). D-BLZ945 had

concentration dependent inhibitory effect and was similar efficacious than free BLZ945 at high concentration of 2000 ng/mL (5000 nM). The same trend was also observed after 24 h co-treatment of IL4 and D-BLZ945 or BLZ945 (B, **Figure 14**). This clearly indicates that D-BLZ945 has therapeutic effect as the free drug.

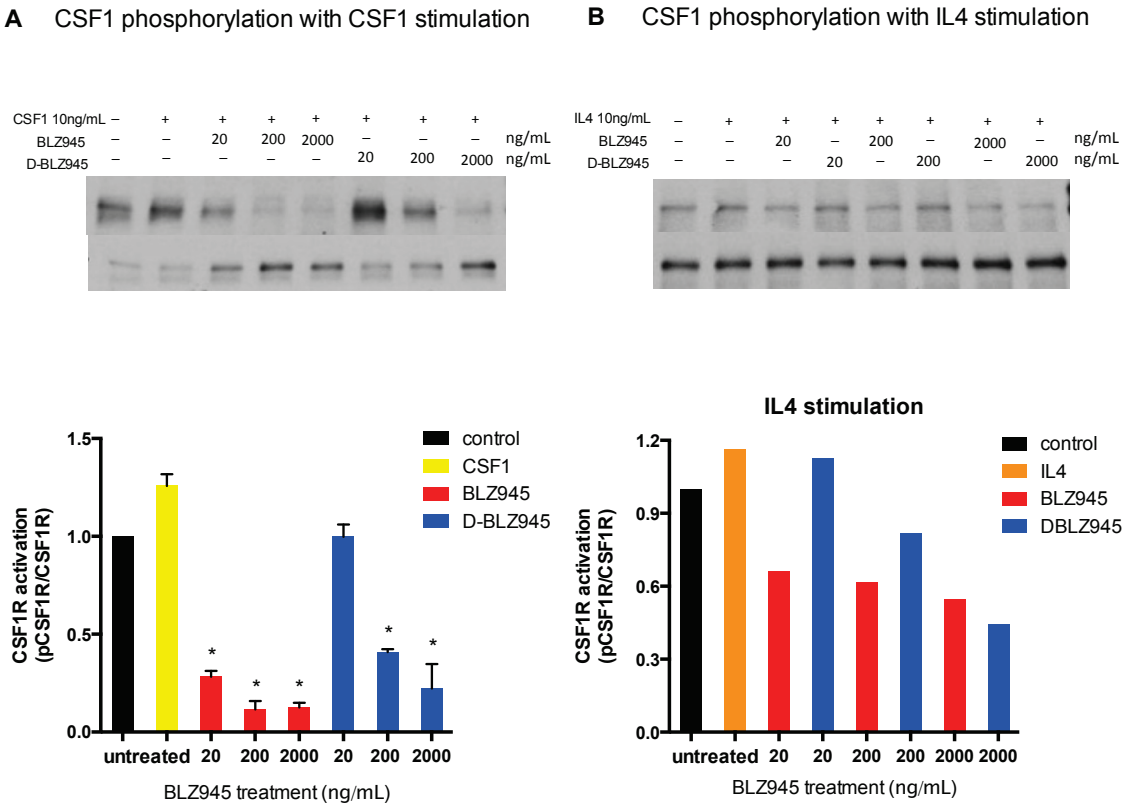

Figure 14 The inhibitory effect of D-BLZ945 on CSF1R phosphorylation in comparison to BLZ945. The upper row was the western blot results and the bottom row was the quantification of the upper graph by normalizing them to the control with arbitrary units. (A) BV2 cells were treated with BLZ945 or D-BLZ945 (20, 200 and 2000 ng/mL) for 12 h prior to changed fresh media and stimulated with CSF1 for 30 minutes. n=3 independent replicates, * compared to CSF1 group, $p<0.05$. (B) BV2 cells were treated with BLZ945 or D-BLZ945 (20, 200 and 2000 ng/mL) for one hour before adding IL4 for 24 h co-incubation.

(3) Inhibitory effect of D-BLZ945 and BLZ945 on IL4 stimulated Arg-1 expression

Previous study showed that CSF1R suppression by BLZ945 reduces M2 macrophage polarization by decreasing M2 markers expression, which leads to the reprogram of tumor

microenvironment and inhibition of tumor growth.[46] To investigate the anti-M2 phenotype effect of D-BLZ945 conjugate, we measured arginase-1 production. The up-regulated expression of arginase-1, a key feature for M2 macrophage, halts the production of NO via inhibiting NOS2 translation and thus initiates anti-inflammatory.[17,20] In the preliminary study, BV2 cells were treated with IL4 (20ng/mL) for 6 h or 24 h (**Figure 15**). Upon 6 hour IL4 treatment, Arg-1 expression was increased and there was a significant increase in Arg-1 expression after 24 h. A lower concentration of IL4 10ng/mL also significantly increased Arg-1 level after 24 h treatment. I further used 10 ng/mL to polarize BV2 cells in the following studies.

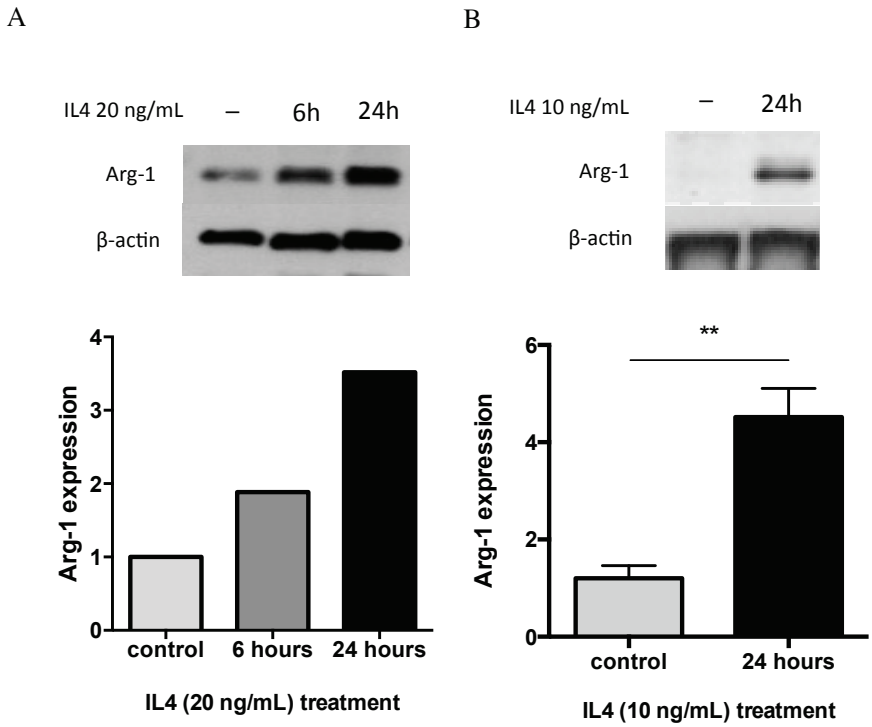

Figure 15 IL4 stimulated Arg-1 expression. The top row was western blot results and the bottom row was the quantification analyses of the upper graphs. (A) BV2 cells were treated with IL4 (20 ng/mL) for 6 h and 24 h. (B) BV2 cells were treated with IL4 (10 ng/mL) for 24 h. n=3 independent replicates. ** p value <0.01.

To study the inhibitory effect of D-BLZ945 and BLZ945 on IL4 induced Arg-1 expression, I first treated cell with D-BLZ945 and BLZ945 for one hour to enable the uptake of drug.

Then IL4 (10 ng/mL) was added to the culture media to stimulate the M2 polarization. BV2 cells were incubated with drug and IL4 for 24 h before collecting proteins. I measured the Arg-1 protein level using western blot. The results showed that D-BLZ945 and free BLZ945 decrease Arg-1 production compared to IL4 treated positive control (**Figure 16**). D-BLZ945 and BLZ945 exhibited dose-dependent manner while no significant difference was observed between 20 ng/mL and 200 ng/mL treatment groups. D-BLZ945 showed more efficacious than BLZ945 in suppressing Arg-1 expression at the same concentration group. Also at the low concentration of 2 ng/mL, D-BLZ945 was observed to reduce Arg-1 level more than BLZ945 (**Figure 17**). G4OH dendrimer vehicle itself had no inhibitory effect. D-BLZ945 seemed to have comparatively better inhibitory effect than free BLZ945. However, average from independent replicates didn't show significant difference between D-BLZ945 and BLZ945.

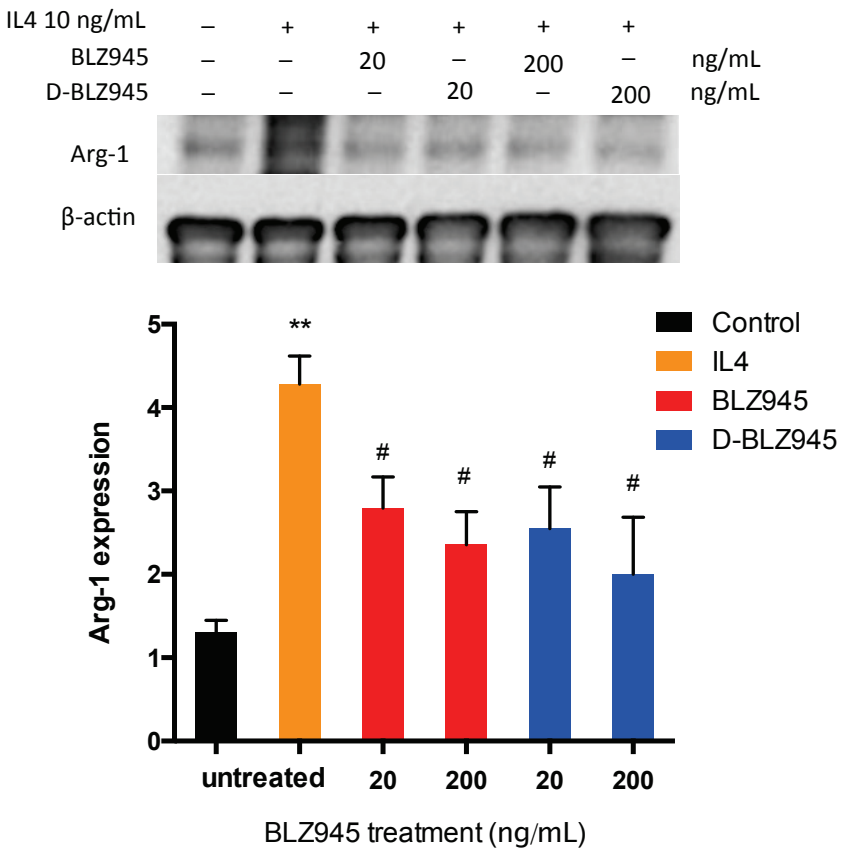

Figure 16 The inhibitory effect of D-BLZ945 and BLZ945 on IL4 induced Arg-1 expression. The top row was western blot results and the bottom row was the quantification analyses of the upper graphs. BV2 cells were treated with BLZ945 or D-BLZ945 (20 ng/mL and 200 ng/mL) for one hour before adding IL4 for 24 h co-incubation. n=4 independent duplicates. ** $p<0.01$; # compared to IL4 treatment group, $p < 0.05$.

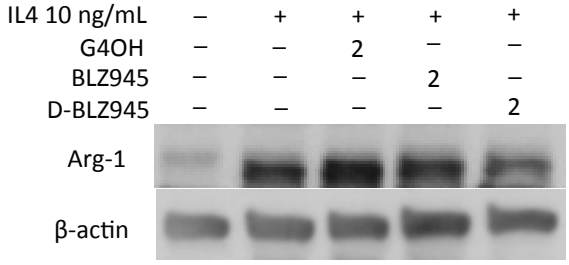

Figure 17 The inhibitory effect of D-BLZ945 and BLZ945 on IL4 induced Arg-1 at low concentration. BV2 cells were treated with BLZ945, D-BLZ945 or G4OH (2 ng/mL) for one hour before adding IL4 for 24 h co-incubation.

3.3.2 *In vitro* efficacy of D-PD98059

PD98059 is a selective inhibitor for MAPK pathway, which gets activated after pro-inflammatory stimulation in macrophages.[30, 41] To investigate the potential anti-inflammatory effect of PD98059 and D-PD98059, we evaluated the pro-inflammatory cytokines (IL1β, IL6, TNFα) expressions at mRNA level. Before drug treatment, we first used LPS to polarize BV2 cells to be pro-inflammatory phenotype and determined the appropriate treatment time of LPS. The result showed that 3 h LPS treatment is the best strategy in increasing the production of these pro-inflammatory cytokines (**Figure 18**). After adding LPS, the pro-cytokine (IL1β, IL6) gene expressions increased dramatically and reached at peaks within 10 h. After reaching peaks, the induction effect of LPS to the cytokines decreased rapidly in 12h and vanished slowly afterward. TNFα has the similar expression trend but less significant. Anti-inflammatory cytokines (IL4, IL10, TGFβ) levels were also measured (B, **Figure 18**). The expression levels were very low compared to pro-inflammatory cytokines after LPS treatment.

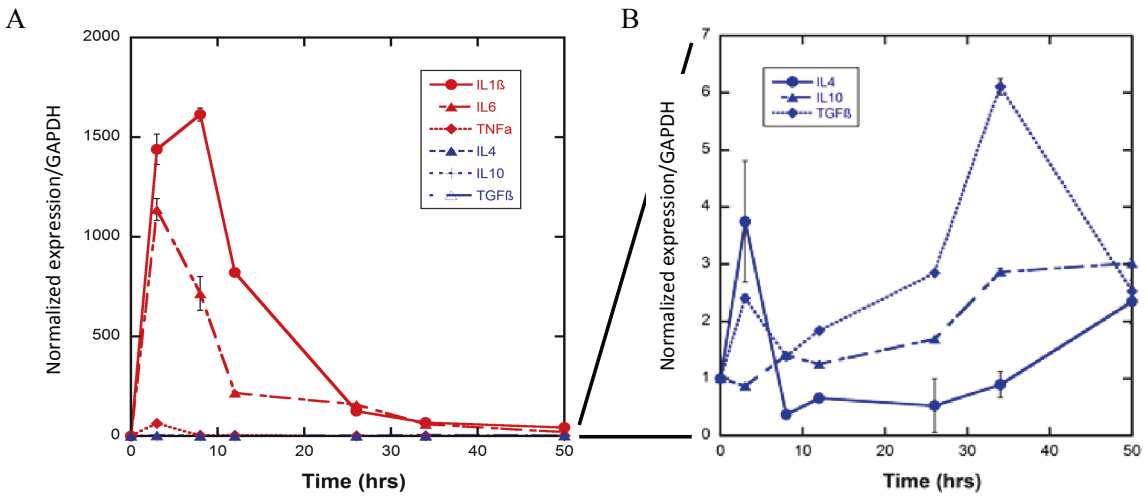

Figure 18 The RNA level of pro-inflammatory cytokines (A) and anti-inflammatory cytokines (B) after LPS stimulation. BV2 cells were treated with LPS (100 ng/mL) and cell samples were collected after different time points to measure the cytokines levels. n=3 independent replicates.

To study the effects of D-PD98059 on the pro-inflammatory cytokines, I activated BV2 cells with LPS for 3 h, following with free PD98059, D-PD98059 and free dendrimer treatment with different doses for 6 or 24 h (**Figure 19**). The results show that 3 h of LPS treatment (100 ng/mL) significantly increases the expression of IL1β and IL6 cytokine level. The expression level TNFα was not increased by LPS stimulation. 6 h treatment with lower dose PD98059 (0.2 μM) further up regulates the pro-inflammatory cytokine genes, while treatment with higher dose PD98059 (10 μM) significantly inhibited the increase of pro-inflammatory cytokines. This trend is reversed when cells are treated with same doses (on PD98059 base) of D-PD98059 for same time span (**Top panel, Figure 19**). Treatment of BV2 cells with D-PD98059 using same doses showed different effects on the pro-inflammatory cytokine genes: low dose of D-PD98059 (0.2 μM) did not affect the pro-inflammatory cytokine genes, interestingly, increase the dose to 10 μM significantly up-regulated the pro-inflammatory cytokine genes. Treatment of BV2 cells with free dendrimer did not induce the increase of pro-inflammatory cytokine genes. This precludes the possibility of free dendrimer stimulating the pro-inflammatory cytokine gene regulation. For 24 h treatment group, similar trends are observed, however, as the effects of LPS treatment reduce almost to its original level, the influence of PD98059 and D-PD98059 treatment on LPS induced cytokine gene change reduces significantly compared with 6 h treatment group (**Bottom panel, Figure 19**). We couldn't give a conclusive explanation for these unexpected data. Considering the low drug release rate of D-PD98059, this conjugate was not a good candidate for further study.

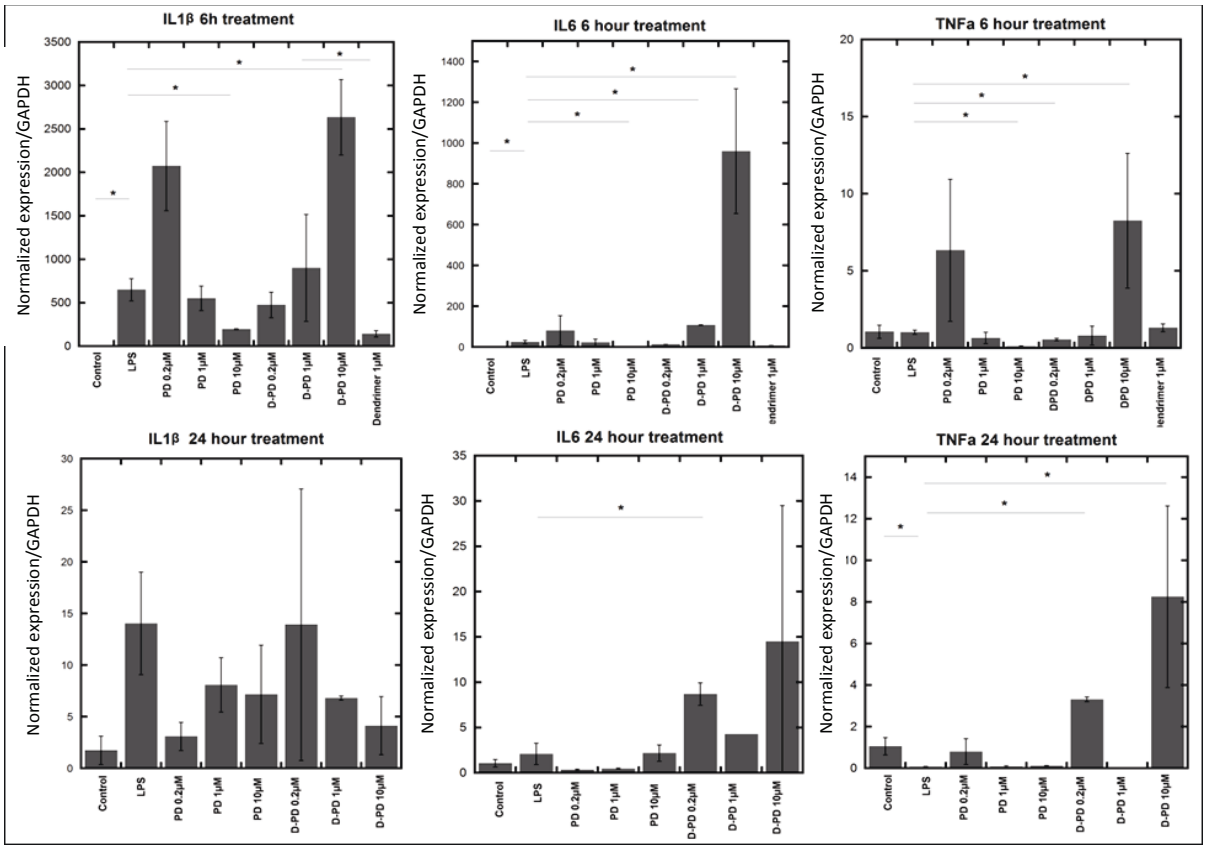

Figure 19 The effect of PD98059 and D-PD98059 on pro-inflammatory cytokine RNA level. Treatment of LPS activates BV-2 cell line with PD98095 (displayed as PD in the figure for brevity) and dendrimer conjugated PD98095 (D-PD) for 6 h shows opposite dose response on pro-inflammatory cytokine expression. IL1β (left column), IL6 (middle column), TNFα (right column); Top panel: cytokine gene expression from 6 h treatment group, Bottom panel: cytokine gene expression from 24 h treatment group. n=3 independent replicates, * $p<0.05$

3.4 Summary

No significant toxicity was observed for D-BLZ945 conjugates and BLZ945 on IL4 activated microglia/macrophage cells. The CSF1R inhibition by D-BLZ945 and BLZ945 leads to the suppression of Arg-1 expression, which is a key feature for M2 macrophages (**Figure 20**). D-BLZ945 exhibits dose-dependent inhibitory effect on CSF1R as free BLZ945 and shows comparatively better Arg-1 suppression efficacy. The inhibitory effect of D-BLZ945 on Arg-1 indicates the possible repolarization ability of D-BLZ945 on M2 macrophages. Future

experiments in distinguishing the phenotype of microglia/macrophages via valuating more cytokine levels could be done to further investigate the potential effect of D-BLZ945 in modifying M2 macrophage polarization. Considering the intrinsic targeting ability of G4OH dendrimer to TAMs in the 9L gliosarcoma and the enhanced solubility,[10] D-BLZ945 conjugate would be a viable formulation for intracellular delivery of BLZ945 to TAMs and have improved therapeutic efficacy. The other dendrimer conjugate D-PD98059 didn't show a clear therapeutic effect in the cellular level evaluation and was not good for further study considering its poor drug release rate.

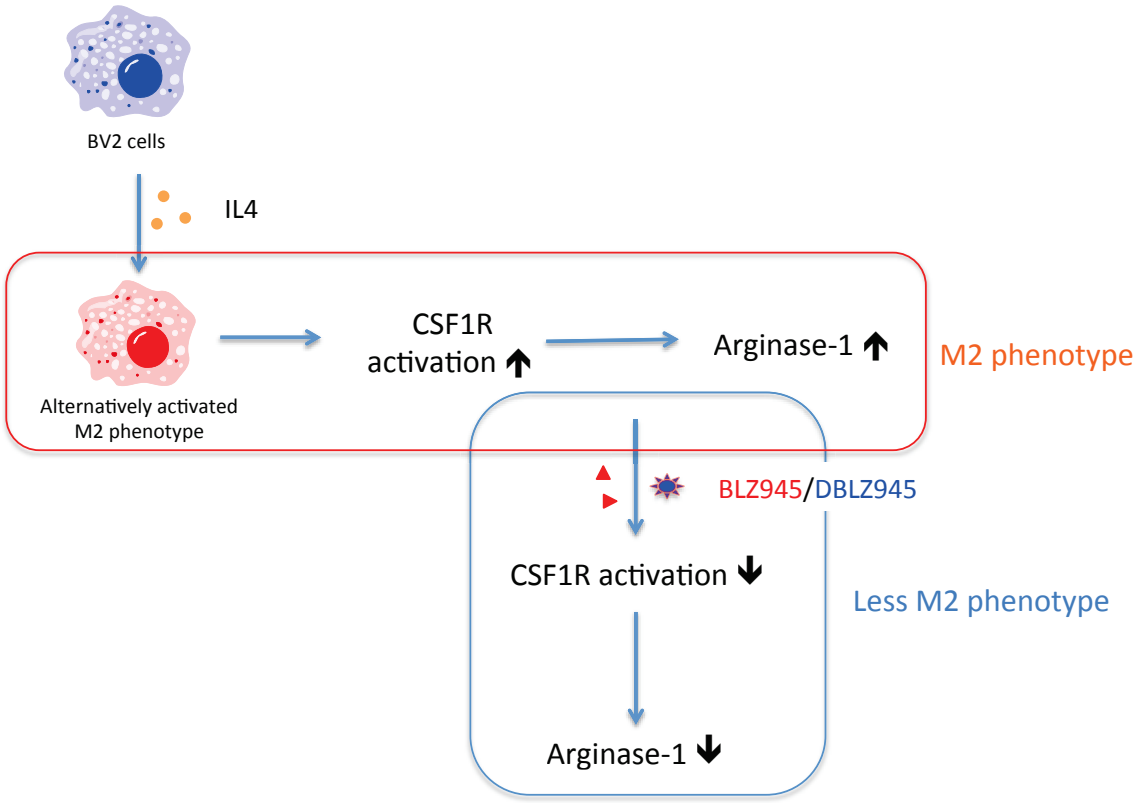

Figure 20 Diagrammatic representations of the mechanism action/hypothesis for *in vitro* efficacy study of D-BLZ945 and BLZ945 on BV2 cells.

Chapter 4: *In vitro* evaluation of the therapeutic efficacy study of Dendrimer-JHU29 conjugates for Rett Syndrome (RTT)

4.1 Introduction

Rett Syndrome (RTT) is a neurological disorder that mainly affects female infants and is most caused by mutations in the methyl-CpG-binding protein 2 gene (MECP2) located on the X chromosome[54]. Inhibition of glutathione (GSH) in activated glial cells induces oxidative stress and underlies the pathogenesis and worsening of symptoms in RTT[55, 56]. More specifically, activated microglial cells (M1 phenotype) and astrocytes express pro-inflammatory cytokines and initiate a neuroinflammation environment that leads to oxidative injury and increased glutamate expression. The excessive glutamate expression and reactive oxygen species in nervous system causes excitotoxicity and injuries to the CNS cells.[57] Many therapeutic strategies have been developed to inhibit neurotoxic microglial activation, including the modulation of extracellular glutamate level by inhibiting microglial glutaminase.[58,59]

Bis-2-(5-phenylacetamido-1,2,4-thiadiazol-2-yl)ethyl sulfide(BPTES) analogs are selective inhibitors of kidney-type GLS modified from insoluble BPTES molecule with multiple enhanced drug properties.[38] JHU29 is a BPTES analog with similar GLS inhibitory potency compared to BPTES. JHU29 inhibits human kidney-type glutaminase with IC_{50} of 2.7 μM, while it showed no inhibition of mouse liver-type glutaminase (GLS2) up to 100 μM.[38] Our lab developed dendrimer-JHU29 (D-JHU29) conjugates and the in vitro anti-glutaminase efficacy of D-JHU29 is evaluated in this chapter. I investigated the cytotoxicity of D-JHU29

on LPS activated microglia cells and measured the extracellular glutamate level to see the glutaminase suppression ability of D-JHU29.

4.2 Methods and materials

4.2.1 Preparation of JHU29 and D-JHU29 formulation for in vitro study

JHU29 (1 mg) was first dissolved in 20 μL DMSO and then added into 980 μL medium to make a 1 mg/mL stock solution. DJHU29 (1 mg) was dissolved in 1 mL medium containing 2 μL DMSO as a 1mg/mL stock solution. These stock solutions were then diluted with fresh phenol-red free DMEM medium into different concentrations for experiment use. The D-JHU29 concentrations were showed in terms of corresponding free JHU29 concentrations in it. D-JHU29 formulations contain same percentage of DMSO as JHU29 in the same concentration groups.

4.3.2 Cell culture for BV2 cells

BV-2 cells were cultured in Dulbecco's modified Eagle's medium (DMEM, Life technologies) with 5 % fetal bovine serum (FBS, Invitrogen) and 1% penicillin-streptomycin (P/S, Invitrogen) at 37 ˚C with 5% CO2 in an incubator.

4.3.3 Cytotoxicity study of JHU29 and D-JHU29

BV2 cells were seeded in 96 well plates with a concentration of 10,000 cells/well (100 μL/well) and incubated for 24 h. Then the cells were treated with culture medium containing LPS (100 ng/mL) and different concentrations (1 μg/mL, 10 μg/mL and 50 μg/mL) of JHU29 and D-JHU29 at increasing concentrations for 24 h. Cell viability was evaluated using MTS cell proliferation assay (Abcam). Absorbance at 490 nm was read using fluorescence

microplate reader (BioTek Instruments). The cell viability was calculated using the equations given in the kit and normalized as percentage relative to control group.

4.3.4 Glutamate release study

BV2 cells were treated with JHU29 or D-JHU29 (1 μg/mL, 10 μg/mL, 50 μg/mL) 30 minutes before adding LPS (100 ng/mL) for 24 hours co-treatment. Then supernatant were collected to measure extracellular glutamate concentration. The supernatants were collected and used to measure extracellular glutamate level. The glutamate level was evaluated using Amplex® Red Glutamic Acid/Glutamate Oxidase Assay Kit (Invitrogen).

4.3 Results and discussion

(1) Cytotoxicity of D-JHU29 and JHU29 on microglia and macrophage

A cytotoxicity study of D-JHU29 and JHU29 was performed on BV2 microglia cells (**Figure 21**). Because I was interested in investigating the anti-glutaminase effect of D-JHU29 on M1 subtype that highly express glutamate, the toxicities of D-JHU29 and JHU29 on LPS activated microglia cells were evaluated to make sure the potential inhibitory efficacies in the following experiments are not from cell death. BV2 were treated with JHU29 or DJHU29 (1 μg/mL, 10 μg/mL and 50μg/mL) 30 minutes before adding LPS (100 ng/mL) for 24 h co-treatment. The results showed that D-JHU29 and JHU29 are non-toxic to LPS activated BV2 microglia cells after 24 h treatment. The cells in D-JHU29 treatment groups showed higher viability than those in JHU29 treatment group.

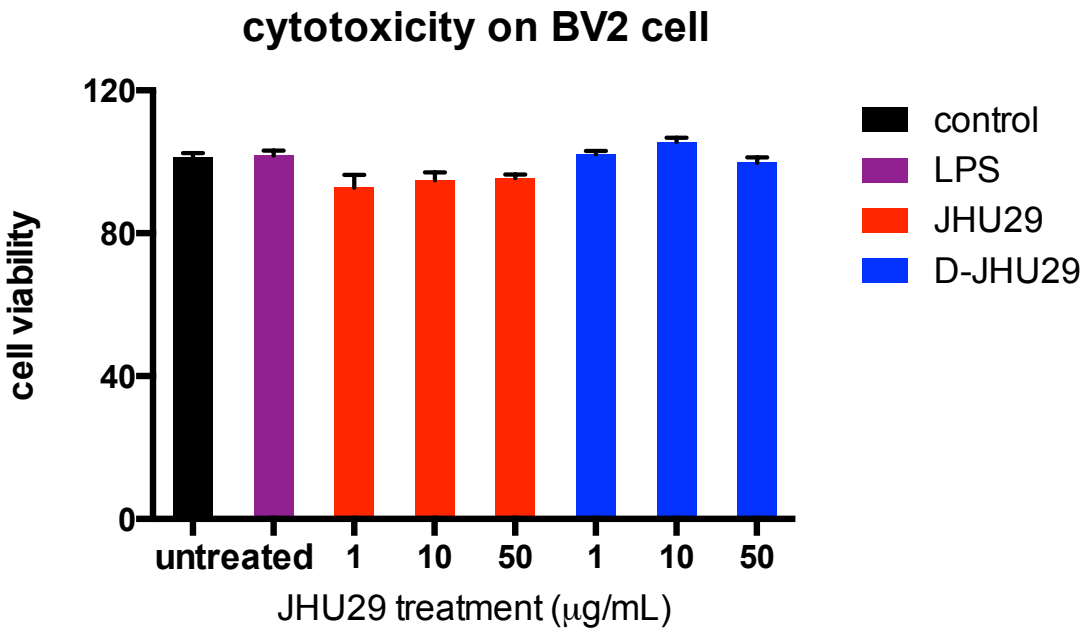

Figure 21 Cytotoxicity of D-JHU29 and JHU29 on LPS activated BV2 cells. BV2 were treated with JHU29 or DJHU29 (1 μg/mL, 10 μg/mL, 50 μg/mL) 30 minutes before adding LPS (100 ng/mL) for 24 h co-treatment. n=6 independent replicates.

(2) The inhibitory effect of D-JHU29 and JHU29 in extracellular glutamate level

The inhibitory effect of free JHU29 drug was first evaluated on BV2 microglia cells. The cells were treated with LPS (100 ng/mL) 30 minutes before adding JHU29 for 24 h co-treatment. The results showed that JHU29 reduce extracellular glutamate level after LPS stimulation in a dose dependent manner. 50 μg/mL JHU29 could down-regulate the glutamate level back to control level.

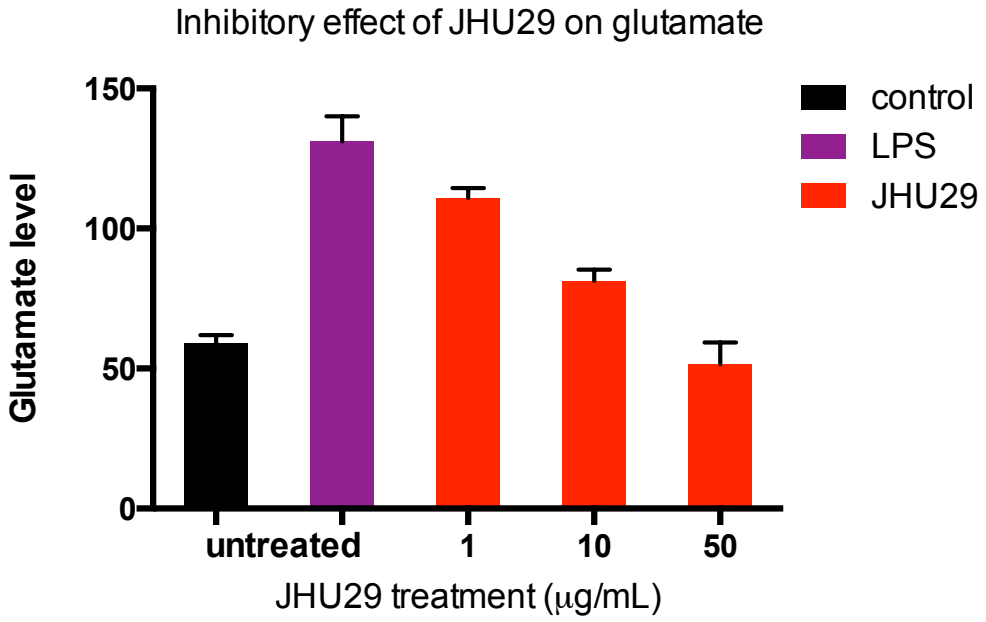

Figure 22 The inhibitory effect of JHU29 on LPS stimulated glutamate expression. JHU29 were added to wells 30 min before adding LPS (100ng/ml) for 24 h treatment. n=3 independent replicates.

The inhibitory effect of D-JHU29 on extracellular glutamate level was then investigated in comparison to JHU29 (**Figure 23**). The results showed that D-JHU29 conjugates reduce LPS stimulated glutamate expression in a dose-dependent manner as JHU29. D-JHU29 and JHU29 of same concentration group had similar effect. It indicates that D-JHU29 was capable of lowering glutamate levels to the same magnitude as free JHU29 and thus had the similar therapeutic efficacy. Considering the targeting ability of G4OH dendrimer, we envision the better therapeutic effect of D-JHU29 in treating neuroinflammation like Rett syndrome.

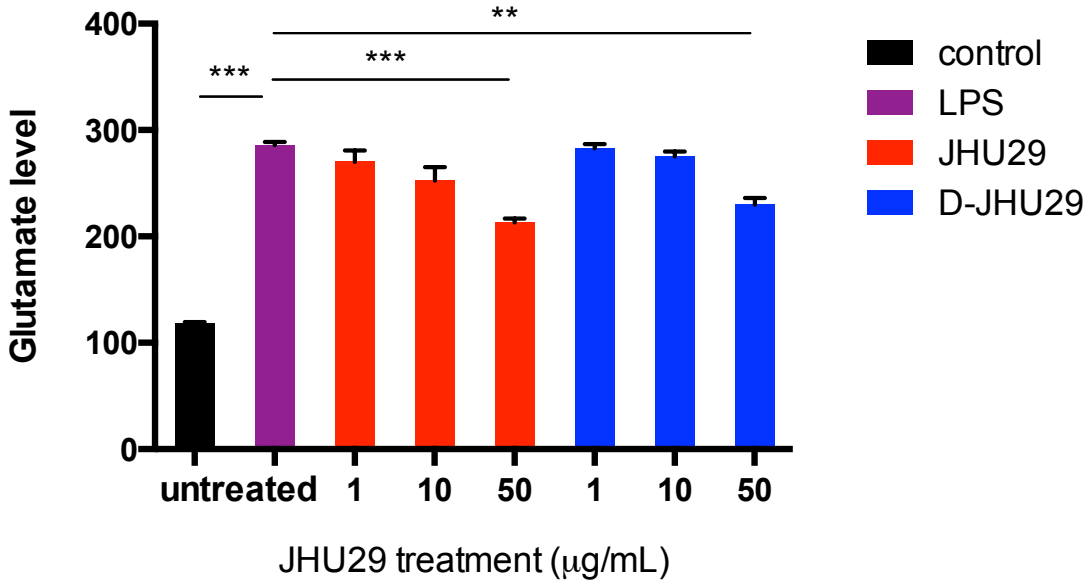

Figure 23 The inhibitory effect of D-JHU29 and JHU29 on extracellular glutamate level. BV2 cells were treated with JHU29 or DJHU29 (1 μg/mL, 10 μg/mL, 50 μg/mL) 30 minutes before adding LPS (100 ng/mL) for 24 h co-treatment. Then supernatant were collected to measure extracellular glutamate concentration. n=3 independent replicates. ***p<0.001; **p<0.01.

4.4 Summary

D-JHU29 is non-toxic to LPS activated microglia cells and the conjugates reduce LPS stimulated glutamate expression in a dose-dependent manner as JHU29. More direct methods to evaluate glutaminase activity may give better indication on its efficacy. Considering the targeting ability of G4OH dendrimer, we envision the better therapeutic effect of D-JHU29 in treating neuroinflammation like Rett syndrome.

Conclusion

In this study, D-BLZ945 and D-PD98059 conjugates were successfully synthesized as potential therapeutic candidates for 9L glioblastoma disease model. The D-PD98059 conjugate showed low drug release rate and didn't have a clear in vitro therapeutic efficacy. By contrast, D-BLZ945 showed potent CSF1R inhibition and Arg-1 suppression effect and may be a promising therapeutic candidate for future study for glioblastoma disease model. D-JHU29 exhibits similar anti-glutaminase efficacy to free JHU29 by measuring extracellular glutamate level. Considering the intrinsic targeting ability of dendrimers and enhanced solubility, dendrimer conjugates (D-BLZ945 and D-JHU29) may be viable formulations for the targeted intracellular delivery of free drugs to improve *in vivo* therapeutic efficacy.

Reference

1. Jain, N. K., V. Mishra, and N. K. Mehra, Targeted drug delivery to macrophages. Expert opinion on drug delivery, 2013. 10(3): p. 353-367.
2. Svenson, S. and D. A. Tomalia, Dendrimers in biomedical applications--reflections on the field. Adv Drug Deliv Rev, 2005. 57(15): p. 2106-29.
3. Menjoge, A. R., R. M. Kannan, and D. A. Tomalia, Dendrimer-based drug and imaging conjugates: design considerations for nanomedical applications. Drug discovery today, 2010. 15(5): p. 171-185.
4. Perumal, O. P., et al., The effect of surface functionality on cellular trafficking of dendrimers. Biomaterials, 2008. 29(24-25): p. 3469-76.
5. Restani, R. B., et al., Biocompatible Polyurea Dendrimers with pH-Dependent Fluorescence. Angewandte Chemie International Edition, 2012. 51(21): p. 5162-5165.
6. Cheng, Y., et al., Polyamidoamine (PAMAM) dendrimers as biocompatible carriers of quinolone antimicrobials: an in vitro study. European journal of medicinal chemistry, 2007. 42(7): p. 1032-1038.
7. Zhang, C., et al., Dendrimer–doxorubicin conjugate as enzyme-sensitive and polymeric nanoscale drug delivery vehicle for ovarian cancer therapy. Polymer Chemistry, 2014. 5(18): p. 5227-5235.
8. Sarin, H., et al., Effective transvascular delivery of nanoparticles across the blood-brain tumor barrier into malignant glioma cells. Journal of translational medicine, 2008. 6(1): p. 80.
9. Mishra, M. K., et al., Dendrimer brain uptake and targeted therapy for brain injury in a large animal model of hypothermic circulatory arrest. ACS nano, 2014. 8(3): p. 2134-2147.
10. Zhang, F., et al., Uniform brain tumor distribution and tumor associated macrophage targeting of systemically administered dendrimers. Biomaterials, 2015. 52: p. 507-516.
11. Kambhampati, S. P., et al., Systemic and Intravitreal Delivery of Dendrimers to Activated Microglia/Macrophage in Ischemia/Reperfusion Mouse Retina. Invest Ophthalmol Vis Sci, 2015. 56(8): p. 4413-24.
12. Quatromoni, J. G. and E. Eruslanov, Tumor-associated macrophages: function, phenotype, and link to prognosis in human lung cancer. Am J Transl Res, 2012. 4(4): p. 376-389.
13. Martinez, F. O., et al., Macrophage activation and polarization. Frontiers in bioscience: a journal and virtual library, 2007. 13: p. 453-461.
14. Mantovani, A., et al., The chemokine system in diverse forms of macrophage activation and polarization. Trends in immunology, 2004. 25(12): p. 677-686.
15. Bronte, V. and P. J. Murray, Understanding local macrophage phenotypes in disease: modulating macrophage function to treat cancer. Nature medicine, 2015. 21(2): p. 117-119.
16. Noy, R. and J. W. Pollard, Tumor-associated macrophages: from mechanisms to therapy. Immunity, 2014. 41(1): p. 49-61.
17. Bronte, V. and P. Zanovello, Regulation of immune responses by L-arginine metabolism. Nature Reviews Immunology, 2005. 5(8): p. 641-654.

18. Coleman, J. W., Nitric oxide in immunity and inflammation. Int Immunopharmacol, 2001. 1(8): p. 1397-406.
19. Mantovani, A., et al., Macrophage polarization: tumor-associated macrophages as a paradigm for polarized M2 mononuclear phagocytes. Trends in immunology, 2002. 23(11): p. 549-555.
20. Lee, J., et al., Translational control of inducible nitric oxide synthase expression by arginine can explain the arginine paradox. Proc Natl Acad Sci U S A, 2003. 100(8): p. 4843-8.
21. Rutschman, R., et al., Cutting edge: Stat6-dependent substrate depletion regulates nitric oxide production. The Journal of Immunology, 2001. 166(4): p. 2173-2177.
22. Lin, E. Y., et al., Colony-stimulating factor 1 promotes progression of mammary tumors to malignancy. The Journal of experimental medicine, 2001. 193(6): p. 727-740.
23. Pixley, F. J. and E. R. Stanley, CSF-1 regulation of the wandering macrophage: complexity in action. Trends in cell biology, 2004. 14(11): p. 628-638.
24. GeneCards, Function for CSF1R Gene. Retrieved from http://www.genecards.org/cgi-bin/carddisp.pl?gene=CSF1R.
25. Zhu, Y., et al., CSF1/CSF1R blockade reprograms tumor-infiltrating macrophages and improves response to T-cell checkpoint immunotherapy in pancreatic cancer models. Cancer research, 2014. 74(18): p. 5057-5069.
26. Strachan, D. C., et al., CSF1R inhibition delays cervical and mammary tumor growth in murine models by attenuating the turnover of tumor-associated macrophages and enhancing infiltration by CD8+ T cells. Oncoimmunology, 2013. 2(12): p. e26968.
27. Pearson, G., et al., Mitogen-activated protein (MAP) kinase pathways: regulation and physiological functions 1. Endocrine reviews, 2001. 22(2): p. 153-183.
28. Chang, L. and M. Karin, Mammalian MAP kinase signalling cascades. Nature, 2001. 410(6824): p. 37-40.
29. Johnson, G. L. and R. Lapadat, Mitogen-activated protein kinase pathways mediated by ERK, JNK, and p38 protein kinases. Science, 2002. 298(5600): p. 1911-2.
30. Rao, K. M. K., MAP kinase activation in macrophages. Journal of Leukocyte Biology, 2001. 69(1): p. 3-10.
31. Agrawal, A. and B. Pulendran, Anthrax lethal toxin: a weapon of multisystem destruction. Cellular and Molecular Life Sciences CMLS, 2004. 61(22): p. 2859-2865.
32. Holcomb, T., et al., Isolation, characterization and expression of a human brain mitochondrial glutaminase cDNA. Molecular brain research, 2000. 76(1): p. 56-63.
33. Erickson, J. W. and R. A. Cerione, Glutaminase: a hot spot for regulation of cancer cell metabolism? Oncotarget, 2010. 1(8): p. 734.
34. Raghavendra Rao, V. L., et al., Traumatic brain injury down-regulates glial glutamate transporter (GLT-1 and GLAST) proteins in rat brain. Journal of neurochemistry, 1998. 70(5): p. 2020-2027.
35. Erdmann, N., et al., Glutamate production by HIV-1 infected human macrophage is blocked by the inhibition of glutaminase. Journal of neurochemistry, 2007. 102(2): p. 539-549.

36. Erdmann, N., et al., In vitro glutaminase regulation and mechanisms of glutamate generation in HIV-1-infected macrophage. Journal of neurochemistry, 2009. 109(2): p. 551-561.
37. Brown, G. C. and A. Vilalta, How microglia kill neurons. Brain Res, 2015. 1628(Pt B): p. 288-97.
38. Shukla, K., et al., Design, synthesis, and pharmacological evaluation of bis-2-(5-phenylacetamido-1, 2, 4-thiadiazol-2-yl) ethyl sulfide 3 (BPTES) analogs as glutaminase inhibitors. Journal of medicinal chemistry, 2012. 55(23): p. 10551-10563.
39. Kannan, S., et al., Dendrimer-based postnatal therapy for neuroinflammation and cerebral palsy in a rabbit model. Science translational medicine, 2012. 4(130): p. 130ra46-130ra46.
40. Wang, B., et al., Anti-inflammatory and anti-oxidant activity of anionic dendrimer-N-acetyl cysteine conjugates in activated microglial cells. Int J Pharm, 2009. 377(1-2): p. 159-68.
41. Alessi, D. R., et al., PD 098059 is a specific inhibitor of the activation of mitogen-activated protein kinase kinase in vitro and in vivo. Journal of Biological Chemistry, 1995. 270(46): p. 27489-27494.
42. Hotokezaka, H., et al., U0126 and PD98059, specific inhibitors of MEK, accelerate differentiation of RAW264. 7 cells into osteoclast-like cells. Journal of Biological Chemistry, 2002. 277(49): p. 47366-47372.
43. Ries, C. H., et al., CSF-1/CSF-1R targeting agents in clinical development for cancer therapy. Curr Opin Pharmacol, 2015. 23: p. 45-51.
44. Ries, C. H., et al., CSF-1/CSF-1R targeting agents in clinical development for cancer therapy. Current opinion in pharmacology, 2015. 23: p. 45-51.
45. Daniel, D., Paradigms for Pre-Clinical Models of Immunotherapy (Powerpoint slides, PDF document), 2015. Retrieved from http://tumor-models.com/wp-content/uploads/sites/67/2015/03/Daniel_Mouse-Models.pdf.
46. Pyonteck, S. M., et al., CSF-1R inhibition alters macrophage polarization and blocks glioma progression. Nature medicine, 2013. 19(10): p. 1264-1272.
47. Hambardzumyan, D., D. H. Gutmann, and H. Kettenmann, The role of microglia and macrophages in glioma maintenance and progression. Nat Neurosci, 2016. 19(1): p. 20-7.
48. Krol, M., et al., Macrophages mediate a switch between canonical and non-canonical Wnt pathways in canine mammary tumors. PLoS One, 2014. 9(1): p. e83995.
49. Niu, M., et al., Tumor-Associated Macrophage-Mediated Targeted Therapy of Triple-Negative Breast Cancer. Mol Pharm, 2016.
50. Zhang, C., et al., Inhibition of tumor growth and metastasis by photoimmunotherapy targeting tumor-associated macrophage in a sorafenib-resistant tumor model. Biomaterials, 2016. 84: p. 1-12.
51. Wan, S., et al., Tumor-associated macrophages produce interleukin 6 and signal via STAT3 to promote expansion of human hepatocellular carcinoma stem cells. Gastroenterology, 2014. 147(6): p. 1393-1404.
52. Fujiwara, N. and K. Kobayashi, Macrophages in inflammation. Current Drug Targets-Inflammation & Allergy, 2005. 4(3): p. 281-286.

53. Wang, M., et al., P38 MAPK mediates myocardial proinflammatory cytokine production and endotoxin-induced contractile suppression. Shock, 2004. 21(2): p. 170-174.
54. Amir, R. E., et al., Rett syndrome is caused by mutations in X-linked MECP2, encoding methyl- CpG-binding protein 2. Nat Genet, 1999. 23(2): p. 185-8.
55. Maezawa, I. and L. W. Jin, Rett syndrome microglia damage dendrites and synapses by the elevated release of glutamate. J Neurosci, 2010. 30(15): p. 5346-56.
56. Derecki, N. C., J. C. Cronk, and J. Kipnis, The role of microglia in brain maintenance: implications for Rett syndrome. Trends Immunol, 2012.
57. Zhao, J., et al., Mitochondrial glutaminase enhances extracellular glutamate production in HIV-1-infected macrophages: Linkage to HIV-1 associated dementia. Journal of neurochemistry, 2004. 88(1): p. 169-180.
58. Potter, M. C., et al., Targeting the glutamatergic system for the treatment of HIV-associated neurocognitive disorders. Journal of Neuroimmune Pharmacology, 2013. 8(3): p. 594-607.
59. Thomas, A. G., et al., Small molecule glutaminase inhibitors block glutamate release from stimulated microglia. Biochemical and biophysical research communications, 2014. 443(1): p. 32-36.

Curriculum Vitae

JIANGYU LI

Baltimore, Maryland 21218
443-310-9329 · jli145@jhu.edu

EDUCATIONAL BACKGROUND

M.S.E. in Biomedical Engineering, Johns Hopkins University, Baltimore, MD
Expected May, 2016; *GPA 3.91/4.0*

B.S. in Marine Pharmacy, China Pharmaceutical University, Nanjing, China
June, 2014; *GPA 90/100*
Scholarship Recipient; Exchange Student with Rutgers University

PROFESSIONAL EXPERIENCE

JOHNS HOPKINS UNIVERSITY — Baltimore, MD

Research Assistant, Center for Nanomedicine (Feb, 2015-May, 2016)
Thesis project: Intracellular delivery of dendrimer-based nanoconjugates for cancer and neuroinflammation
Advisor: Dr. Rangaramanujam M. Kannan

Research Assistant, Calcium Signals Lab (Oct, 2014-Feb, 2015)
Project: Engineer Calcium channels to explore the membrane binding mechanism.
Advisor: Dr. David T. Yue

Teaching Assistant (Aug, 2014-May, 2016)

Serve as TA for BME Modeling and Design, Models and Simulations, and SBE I & II Lab sections.

RUTGERS UNIVERSITY — New Brunswick, NH

Student Researcher/Exchange student, School of Pharmacy, Center for Cancer Prevention Research (Jan, 2014 to June, 2014)
Undergraduate thesis project: Investigate the effect of Gemini Vitamin D analog BXL0124 and 1α,25(OH)2D3 on breast cancer cells
Advisor: Dr. Nanjoo Suh

CHINA PHARMACEUTICAL UNIVERSITY — Nanjing, China

Research Assistant (Oct, 2011 to Jan, 2014):
Projects including: 1) Investigated the effect of traditional Chinese medicine, rhynchophylline, in repairing vascular endothelial cells to treat blood vessel injury. 2) Explored the antioxidant and immune activity of polysaccharide extracted from clam. 3)Performed protein separation and purification for diabetes research. 4) Implemented 3D reconstruction of CT scans using MATLAB

PUBLICATIONS AND PATENTS

Jiangyu Li. 2013. A self-regulated medicine bottle for controlling the quantity of drained-out liquid. Chinese patent No. CN203329038U

Jiangyu Li. 2013. A novel pen-based portable timer. Chinese patent No. CN203338017U

Haiyan Chen*, Bowen Li, Jiadan Qiu, **Jiangyu Li,** Jing Jin, Shuhang Dai, Yuxiang Ma, Yueqing Gu*, Thermal Responsive Micelles for Dual Tumor-targeting Imaging and Therapy. Nanoscale, 2013, 5: 12409–12424.

HONORS AND AWARDS

National Scholarship of China for the highest academic average (twice)	0.2%
Daewoong Scholarship for excellent senior students	<1%
First Class scholarship at China Pharmaceutical University (twice)	<4%
Excellent college graduate	10%